ALMA Science:
a review of (sub)mm band science and instruments in the ALMA era

Marcella Massardi
INAF- Istituto di Radioastronomia
Italian node of European ALMA Regional Centre

ALMA

EUROPEAN ARC
ALMA Regional Centre || Italian

SISSA – February 2014

Why should I go (sub)mm?

The signals

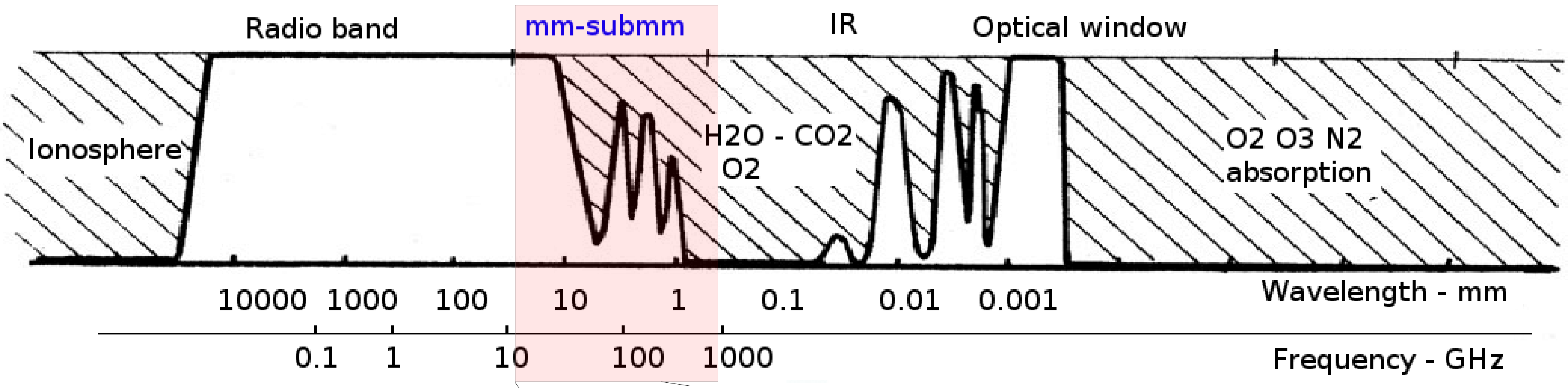

The (sub)mm band ranges between 30-1000 GHz

(Sub)mm signals: synchrotron, dust emission, molecular lines, CMB

- Includes the “cosmological windows”
- CIB constitutes about 50% of galaxy emissions
- Of this, 70% is due to dust
- **Molecular clouds are associated to structure formation and dense regions**
- In (sub)mm there is the peak of dust emission up to high z (negative k correction)
- Extinction is large in molecular clouds at NIR and optical bands but not in (sub)mm

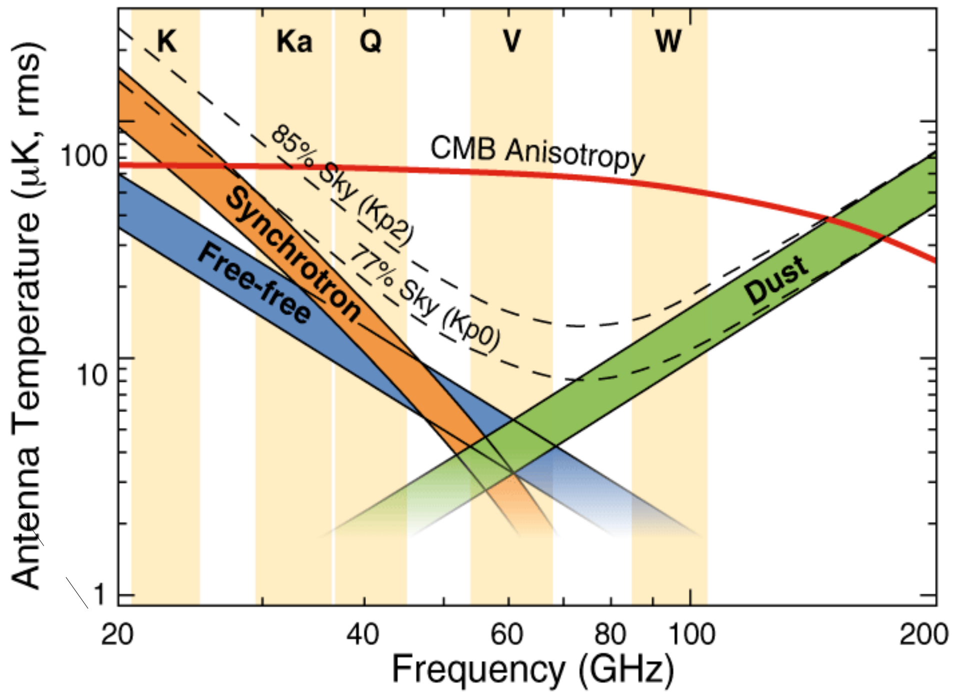

The signals

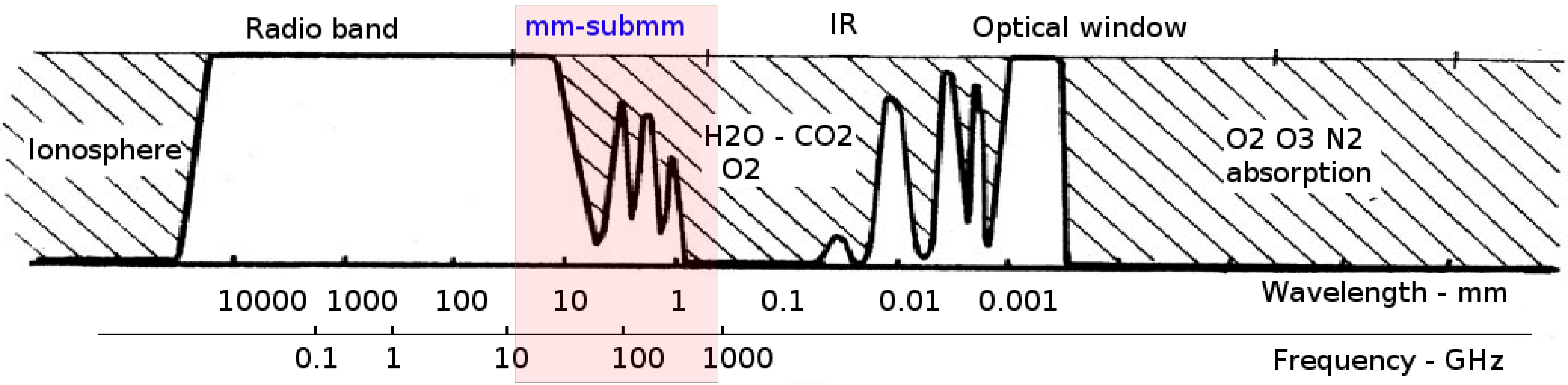

The (sub)mm band ranges between 30-1000 GHz

(Sub)mm signals: synchrotron, dust emission, molecular lines, CMB

- Includes the “cosmological windows”
- CIB constitutes about 50% of galaxy emissions
- Of this, 70% is due to dust
- **Molecular clouds are associated to structure formation and dense regions**
- In (sub)mm there is the peak of dust emission up to high z (negative k correction)
- Extinction is large in molecular clouds at NIR and optical bands but not in (sub)mm

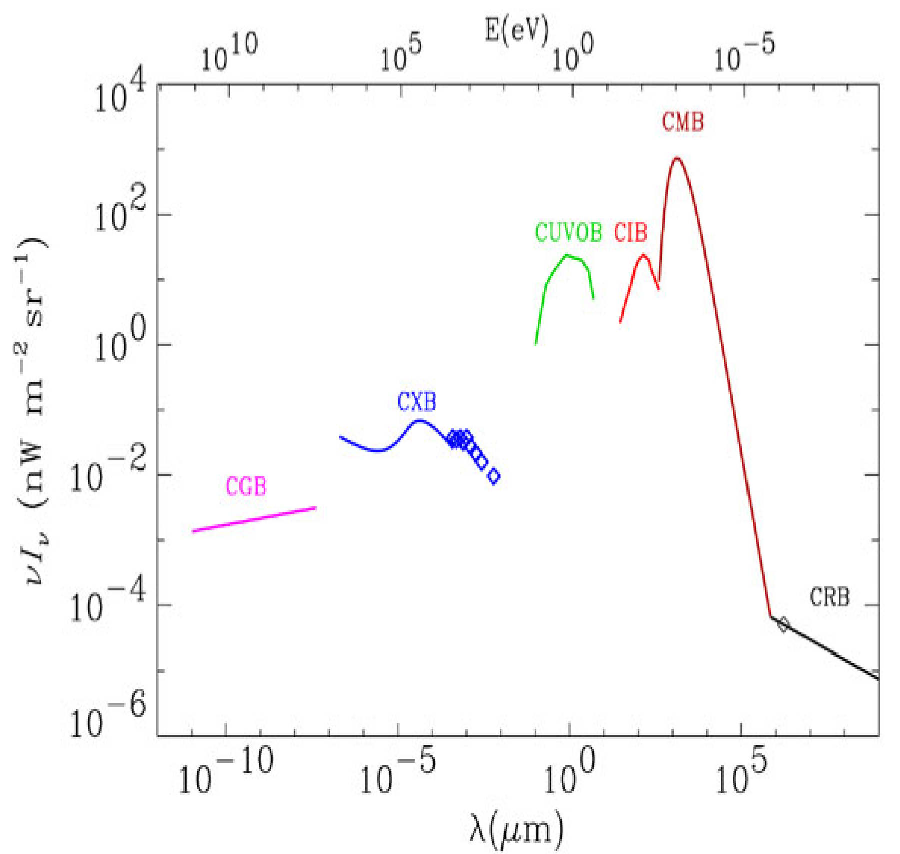

The instruments

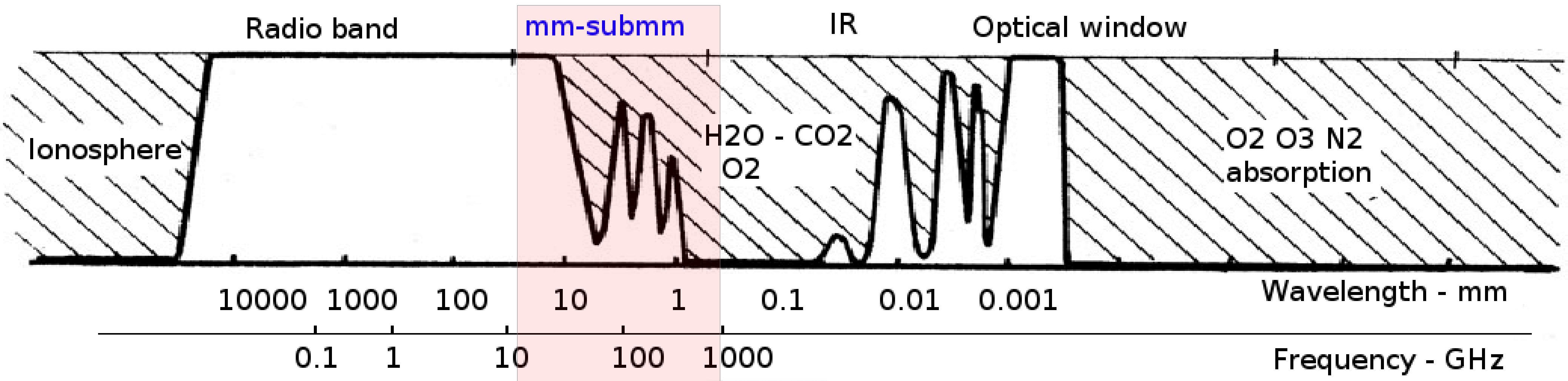

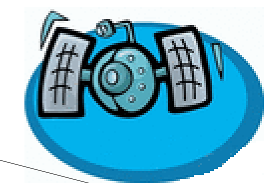

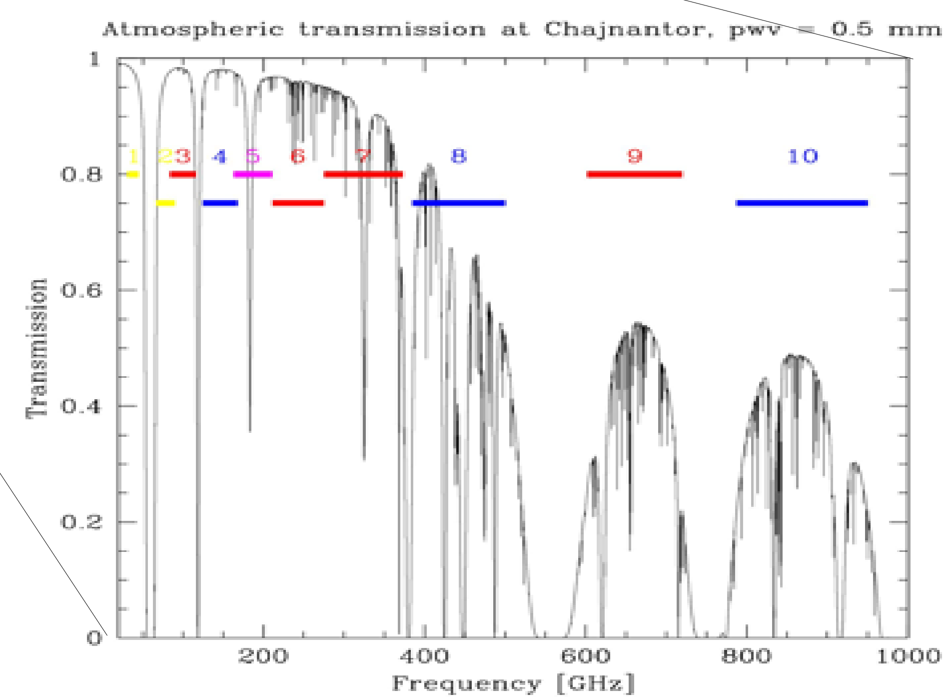

Requirements: Excellent weather
Accurate antennas
Sensitive receivers

Most typically it is observed from space/balloons but few transmissivity bands are allowed also from the ground in dry sites.

Allows higher resolution than radio bands

Outline

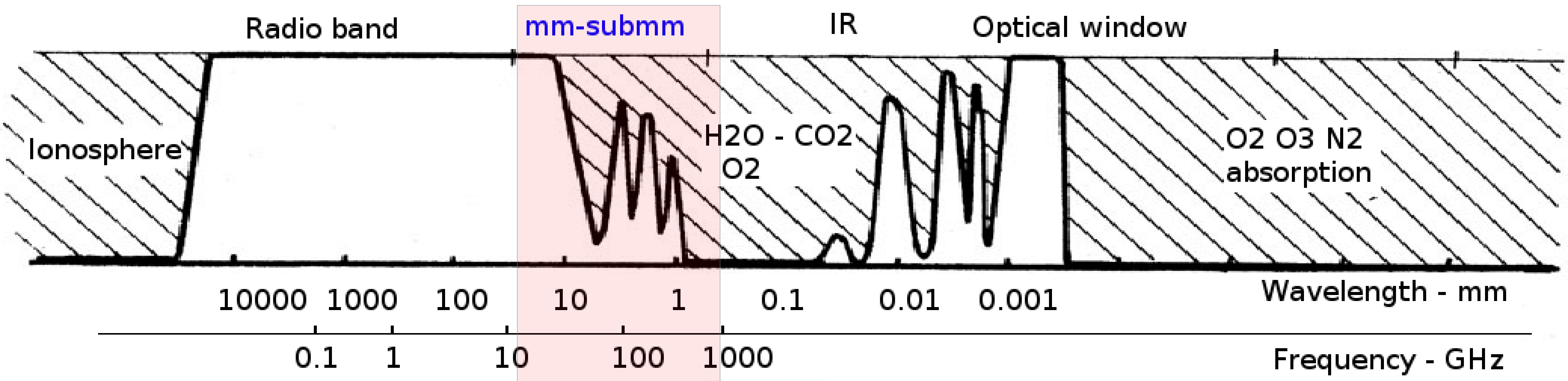


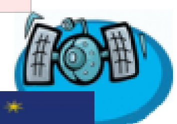

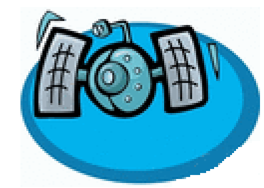

Signals in (sub)mm band — What can we get out of them?

The reasons for ALMA — Pills of interferometry
ALMA properties
Writing a proposal

Galactic Science — From planets to our Galaxy

Extragalactic Science — AGNs
Submm galaxies
Galaxy clusters

The signals

- Introduction to Millimeter/Sub-millimeter Astronomy, T. Wilson, 2009
- Tools of Radioastronomy, K. Rohlfs & T. Wilson, Springer

Some background

The power of an electromagnetic wave passing through an infinitesimal surface is

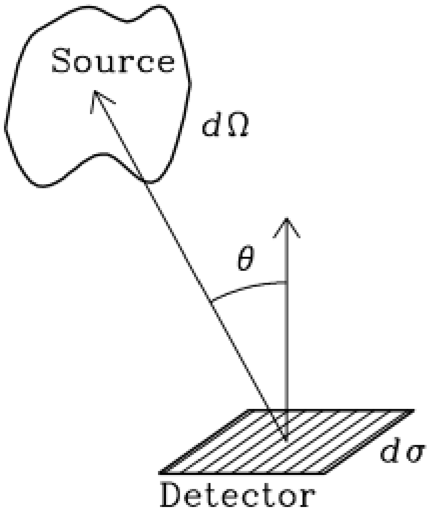

$$\mathrm{d}P = I_\nu \cos\theta \, \mathrm{d}\Omega \, \mathrm{d}\sigma \, \mathrm{d}\nu$$

$\mathrm{d}P$ = power, in watts,
$\mathrm{d}\sigma$ = area of surface, m^2,
$\mathrm{d}\nu$ = bandwidth, in Hz,
θ = angle between the normal to $\mathrm{d}\sigma$ and the direction to $\mathrm{d}\Omega$,
I_ν = brightness or specific intensity, in $\mathrm{W\,m^{-2}\,Hz^{-1}\,sr^{-1}}$.

The total flux is the integral of dP over the solid angle subtended by the source

$$S_\nu = \int_{\Omega_s} I_\nu(\theta,\varphi)\cos\theta \, \mathrm{d}\Omega,$$

Flux density is measured in Jansky

$$1\,\mathrm{Jy} = 10^{-26}\,\mathrm{W\,m^{-2}Hz^{-1}} = 10^{-23}\,\mathrm{erg\,s^{-1}cm^{-2}Hz^{-1}}$$

Brightness does not depend on distance d, while flux density scales as $1/d^2$

Some background

The brightness distribution for a black body in thermal equilibrium with the medium is a Planckian

$$B_\nu(T) = \frac{2h\nu^3}{c^2}\frac{1}{e^{h\nu/kT}-1}$$

In **Rayleigh-Jeans regime**

$$h\nu \ll kT$$

Brightness is proportional to temperature

$$B_{\mathrm{RJ}}(\nu,T) = \frac{2\nu^2}{c^2}kT$$

Define the **radiation temperature**

$$J(T) = \frac{c^2}{2k\nu^2}I = \frac{h\nu}{k}\frac{1}{e^{h\nu/kT}-1}$$

Hence RJ holds for frequencies

$$\frac{\nu}{\mathrm{GHz}} \ll 20.84\left(\frac{T}{\mathrm{K}}\right)$$

Some background

Hence **RJ holds for frequencies** $$\frac{\nu}{\mathrm{GHz}} \ll 20.84 \left(\frac{T}{\mathrm{K}}\right)$$

Thermal sources in (sub)mm are in RJ regime

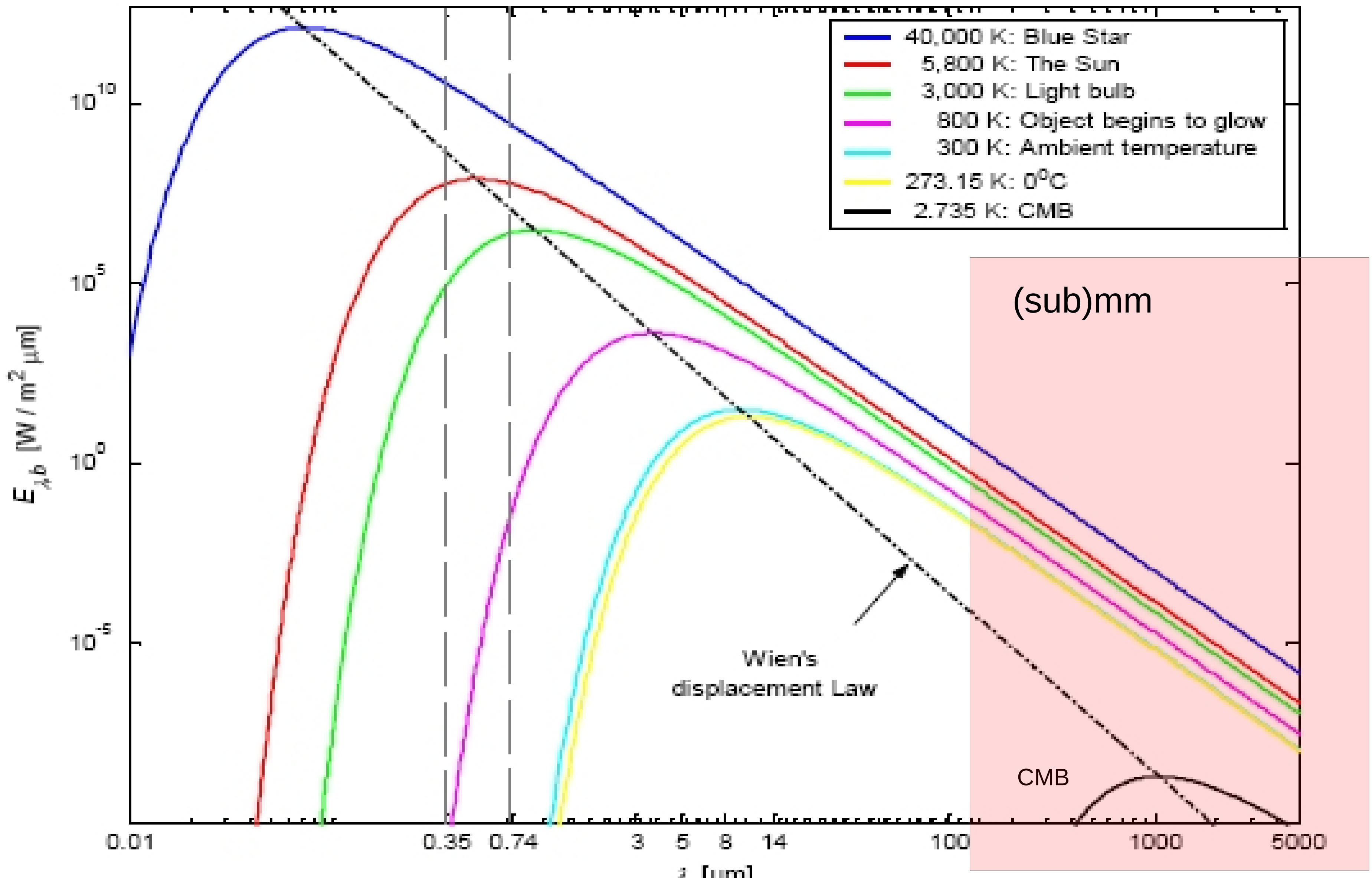

CMB

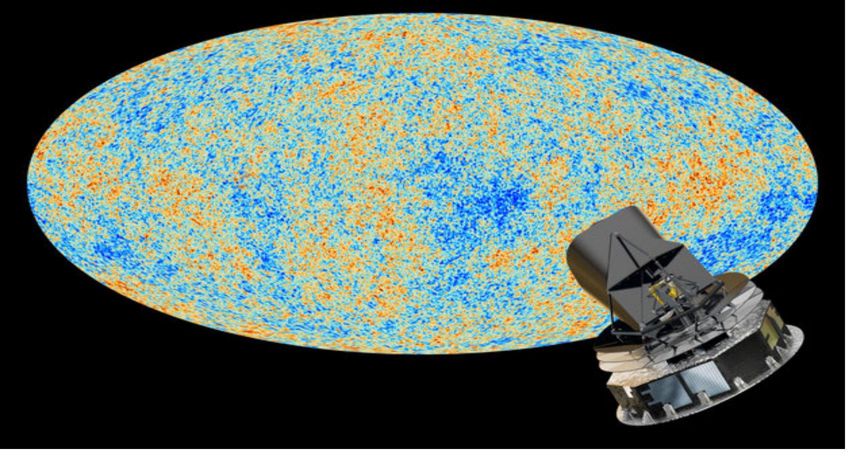

Radiation permeating all the universe at 2.726K
Hence peaking at ~163 GHz
The millimetric band is a cosmologic window because **at the minimum of the intervening foregrounds between the CMB and us.**
Point EG sources are the major contaminant to scales smaller than 30 arcmin.

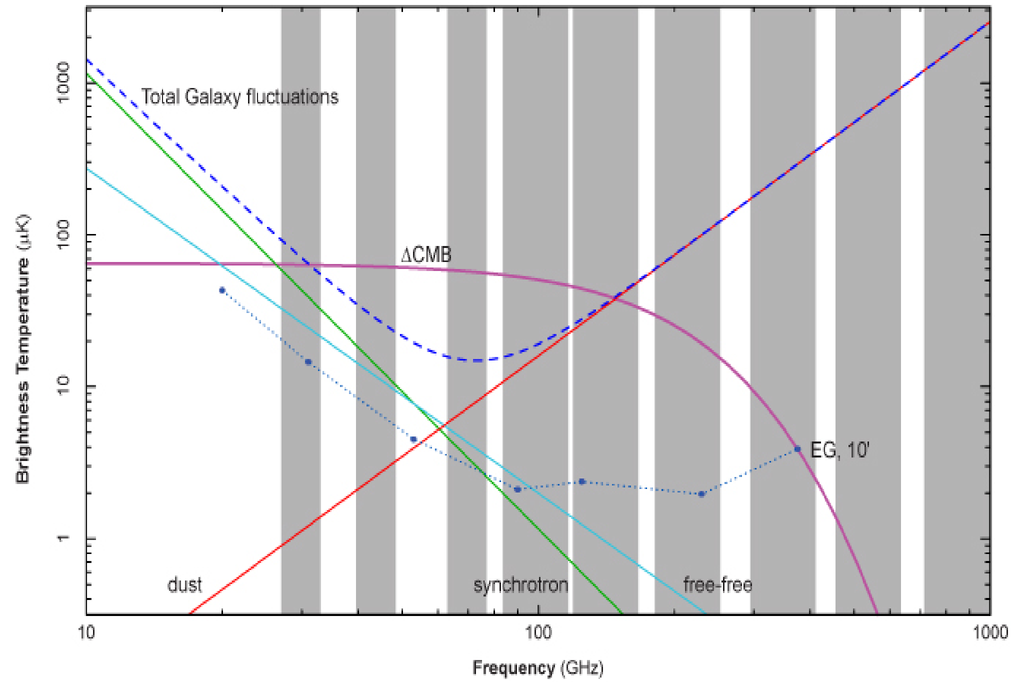

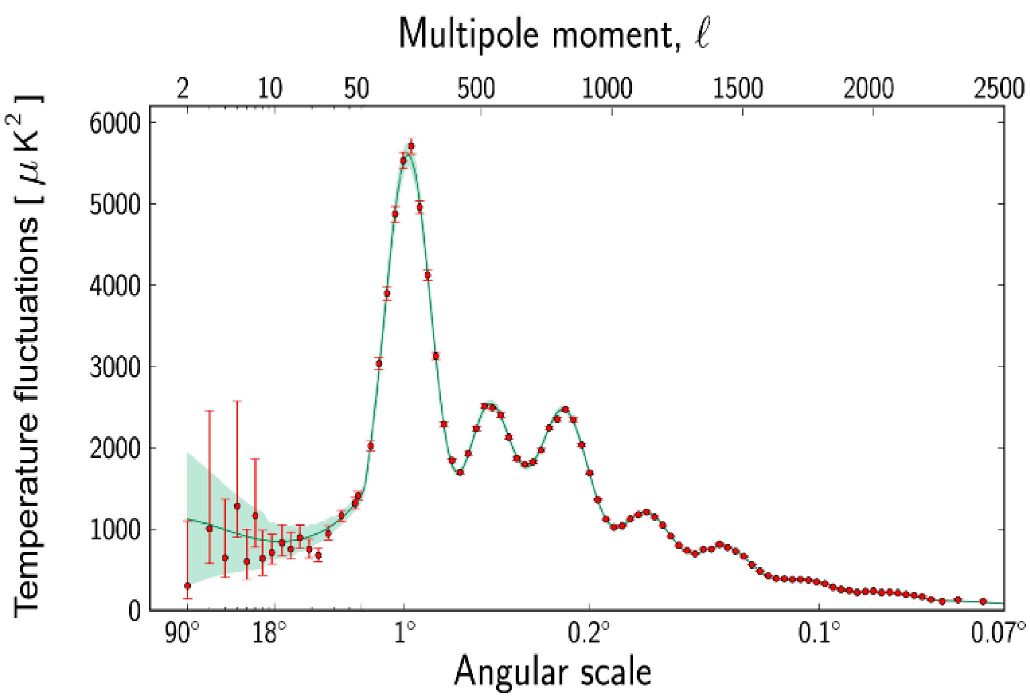

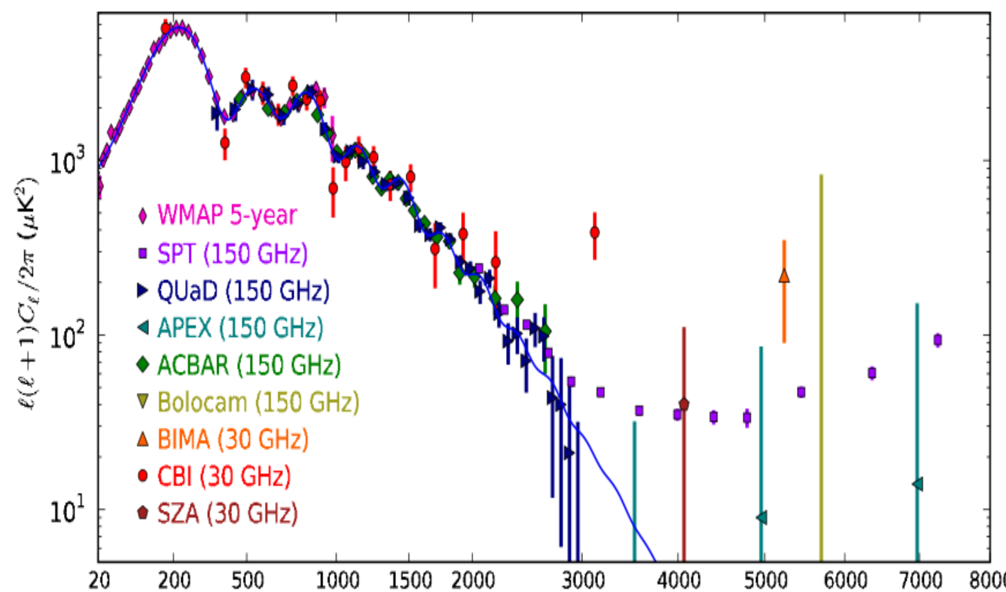

(Fowler et al. 2010, Planck collaboration 2013)

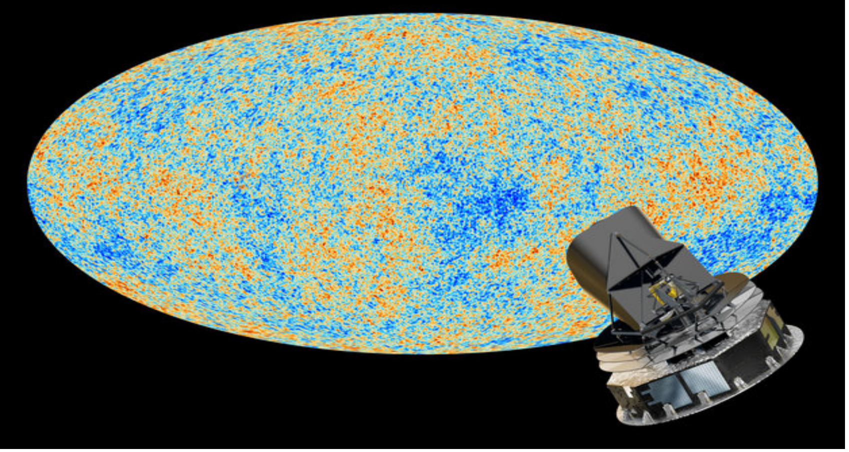

CMB

Radiation permeating all the universe at 2.726K
Hence peaking at ~163 GHz
The millimetric band is a cosmologic window because **at the minimum of the intervening foregrounds between the CMB and us.**
Point EG sources are the major contaminant to scales smaller than 30 arcmin.

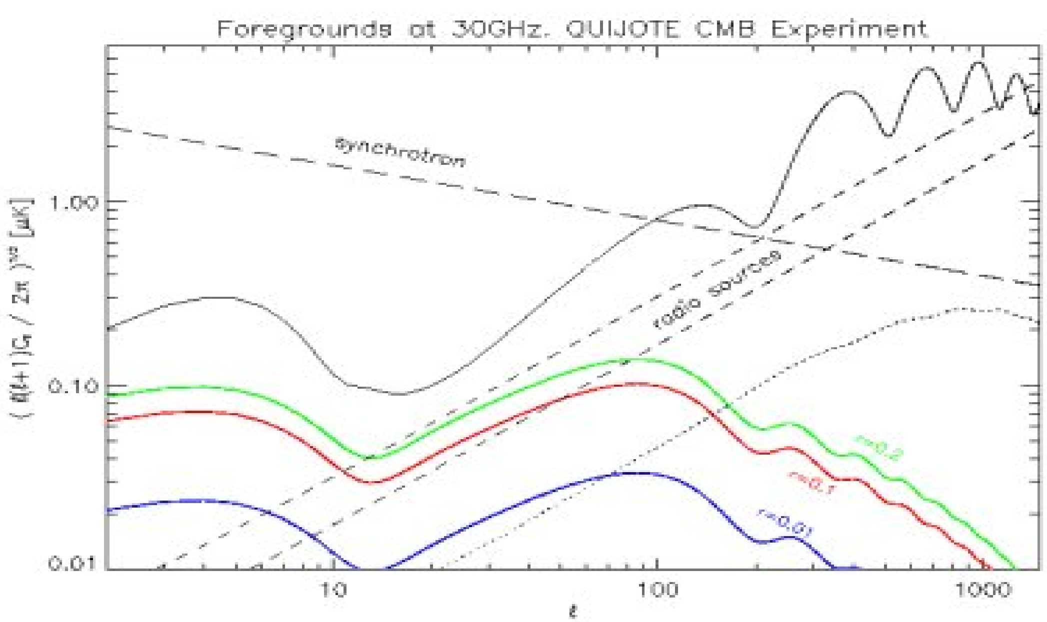

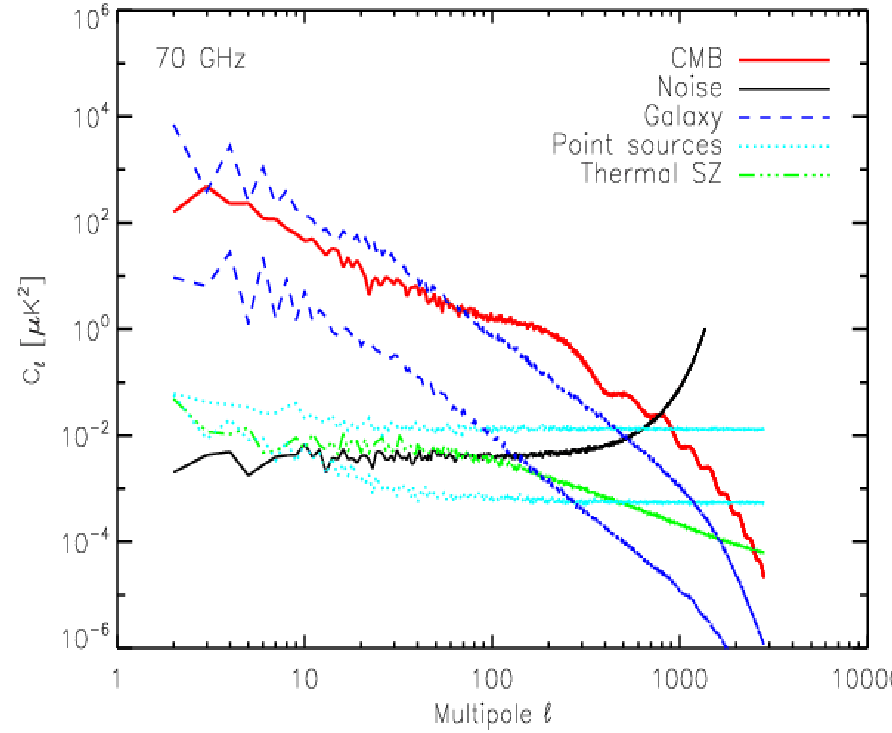

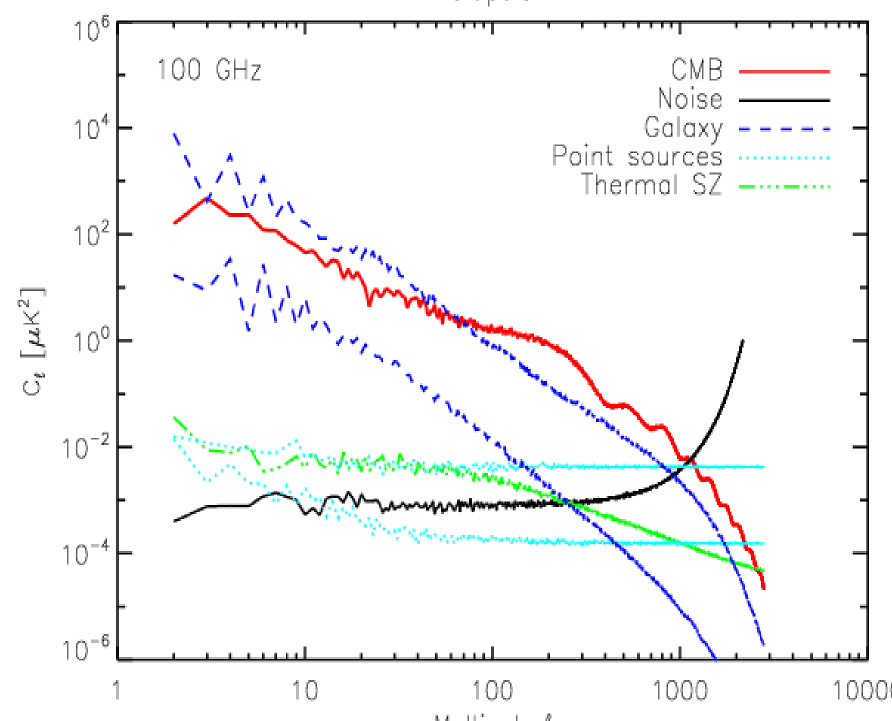

(QUIXOTE website, Leach et al. 2008)

Synchrotron

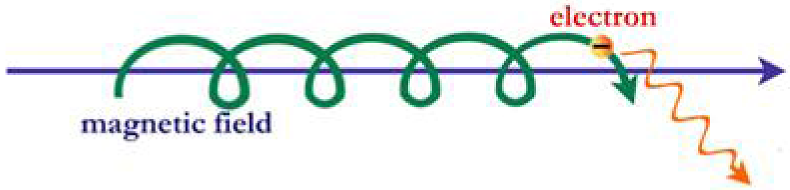

Synchrotron emission is caused by emission from relativistic electrons spiralling in magnetic fields. The radiation emitted is confined to a beam pointing In the direction of the motion of the particle **It is also polarized** in the plane perpendicular to the magnetic field, with the degree and orientation of the polarization providing information about the source magnetic field.

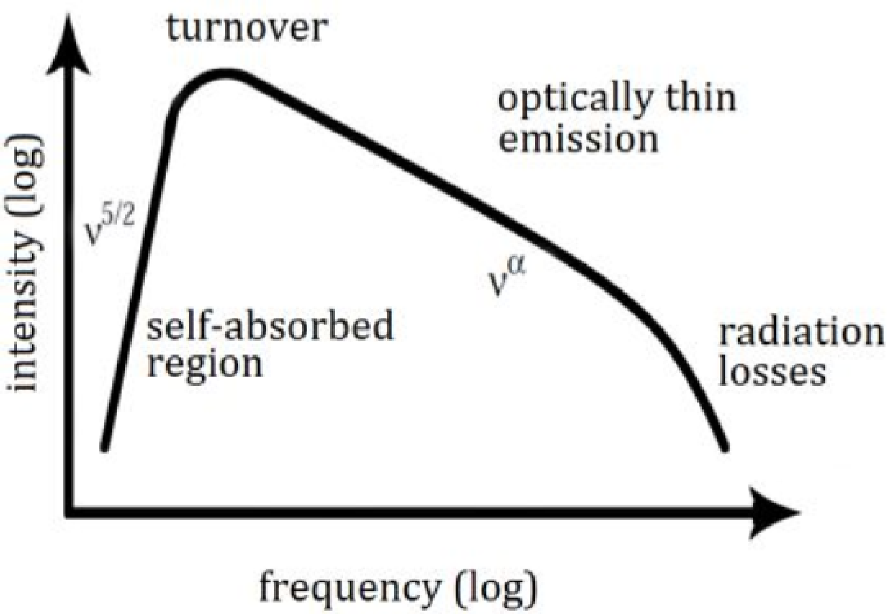

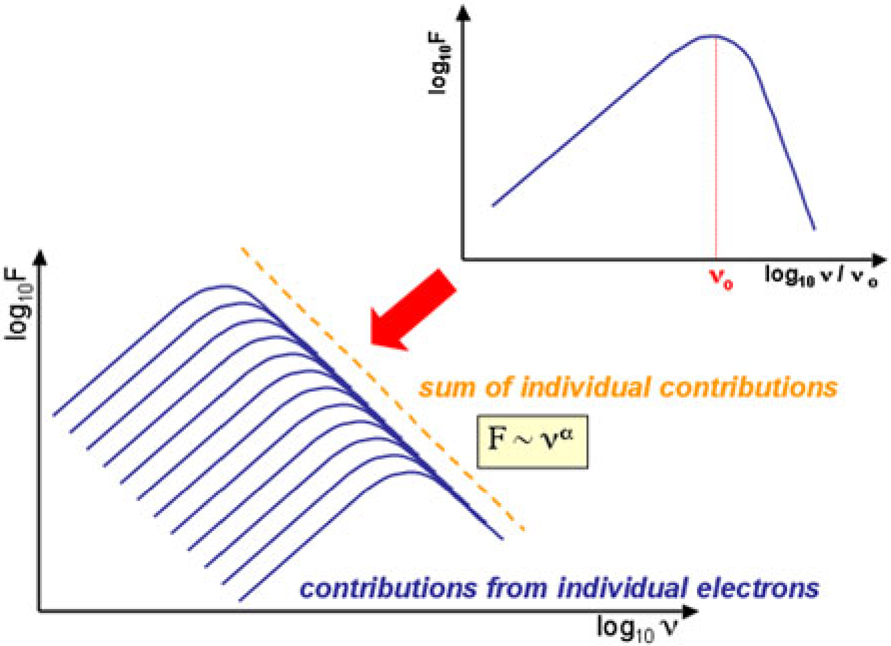

$$\alpha(\nu_1, \nu_2) = \frac{\log(S_1/S_2)}{\log(\nu_1/\nu_2)}$$ **Spectral index**

Synchrotron in AGN

Synchrotron emission is associated to jets in AGN.
Spectral Energy distribution (SED) is a combination of

- **combination of multiple synchrotron components** along the jets with peak at the higher frequencies the more energetic is the emitted photons (i.e. the stronger is the magnetic field = the closer to the BH). More energetic photons are also less absorbed (i.e. electron clouds are less thick). Combined spectra are flatter than the spectra of single components

Steep spectra = synchrotron optically thin emitted
Flat spectra = synchrotron self-absorbed multiple components

- **Doppler boosting** due to relativistic beaming effects that enhances the flux as $S_r = S_e D^{3-\alpha}$ so that in the optically thin regime the flux density increases more than in the thick range.

At higher frequencies the signal is less absorbed and boosted, so the bright samples are dominated by flat spectra sources.

The self-absorbed components are frequently unstable, young and rapidly evolving. Variability affects source counts (we detect more easily high states), SEDs and extrapolations.

Synchrotron in AGN

A sample of S>500mJy mm-band selected sources dominated by flat spectrum objects (but steeper than at lower frequencies).

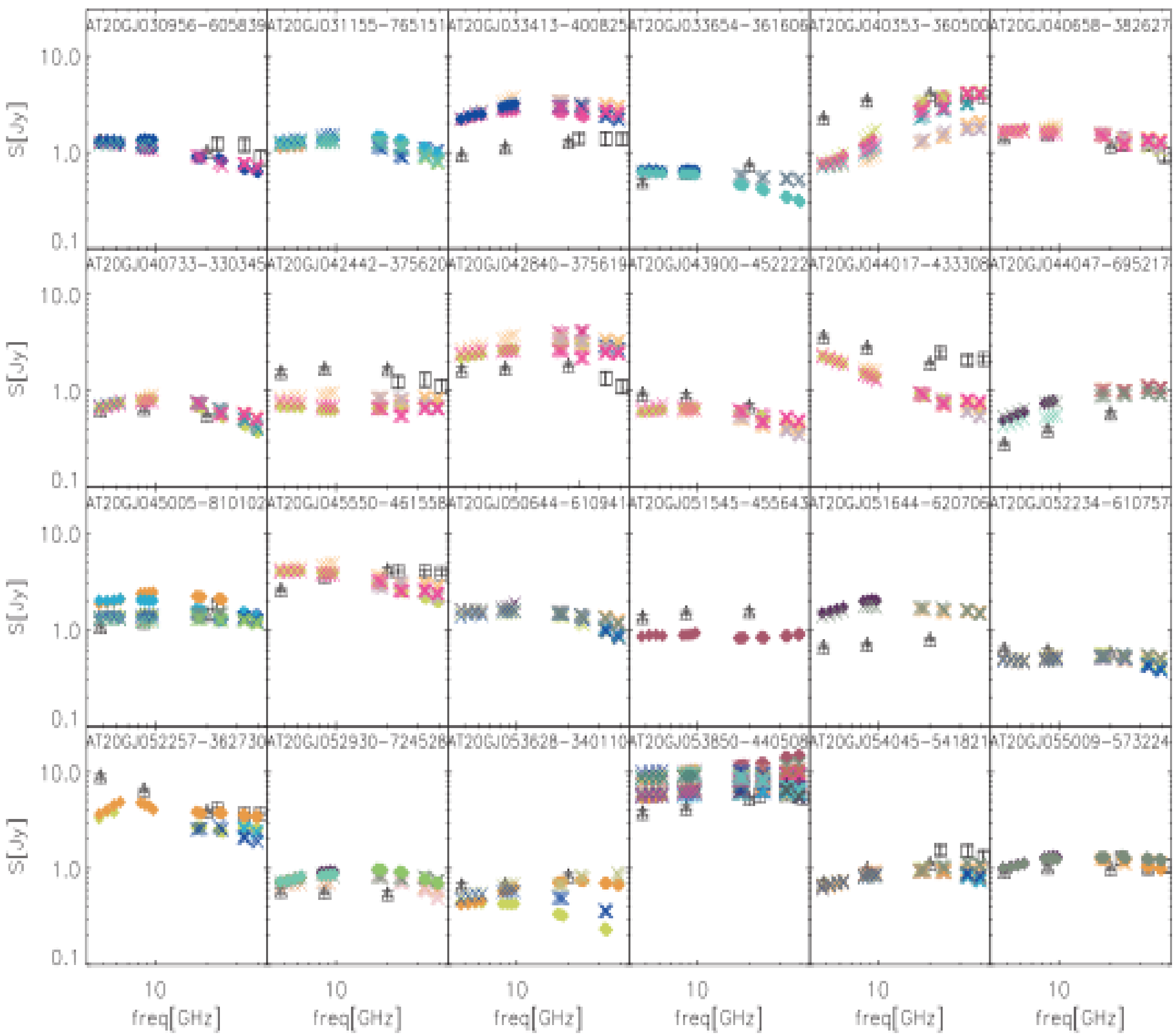

Radio colour-colour plot (comparison between spectral indices)

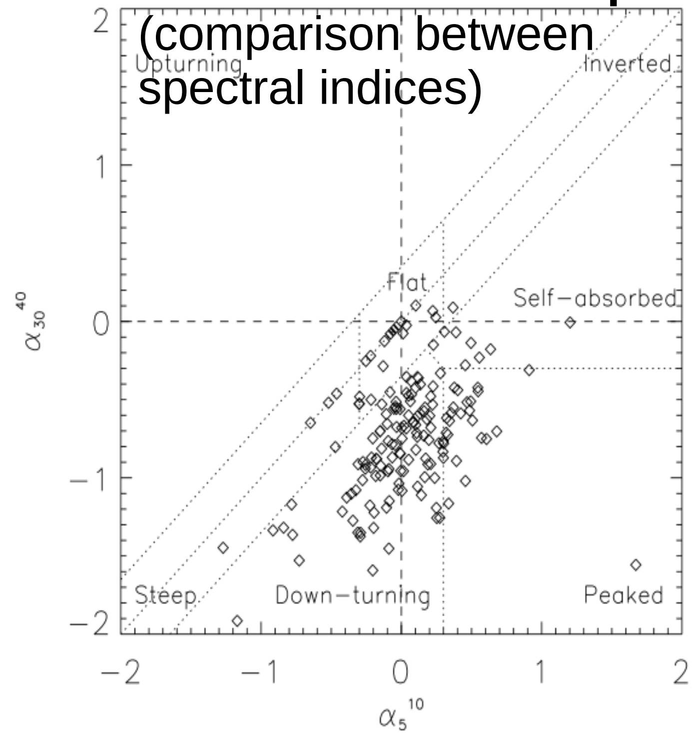

Variability

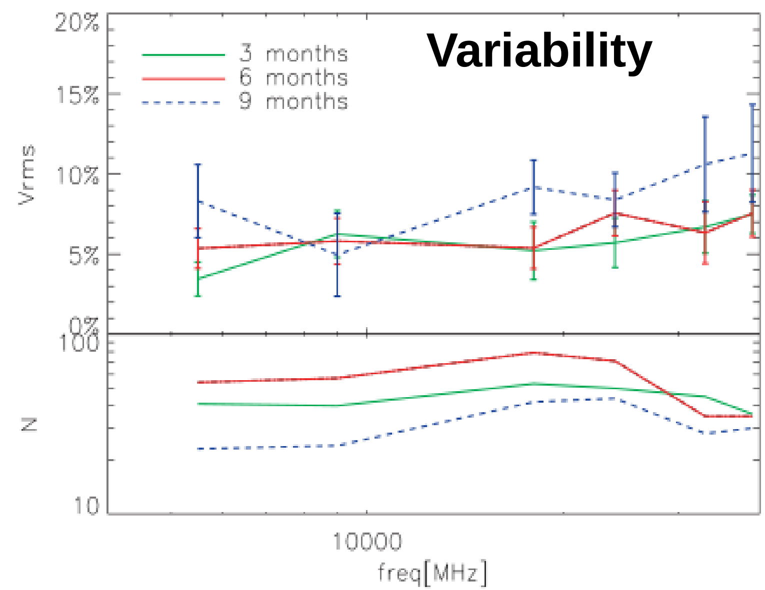

Synchrotron in AGN

A sample of S>200mJy mm-band selected sources dominated by flat spectrum objects (but steeper than at higher flux density selections).

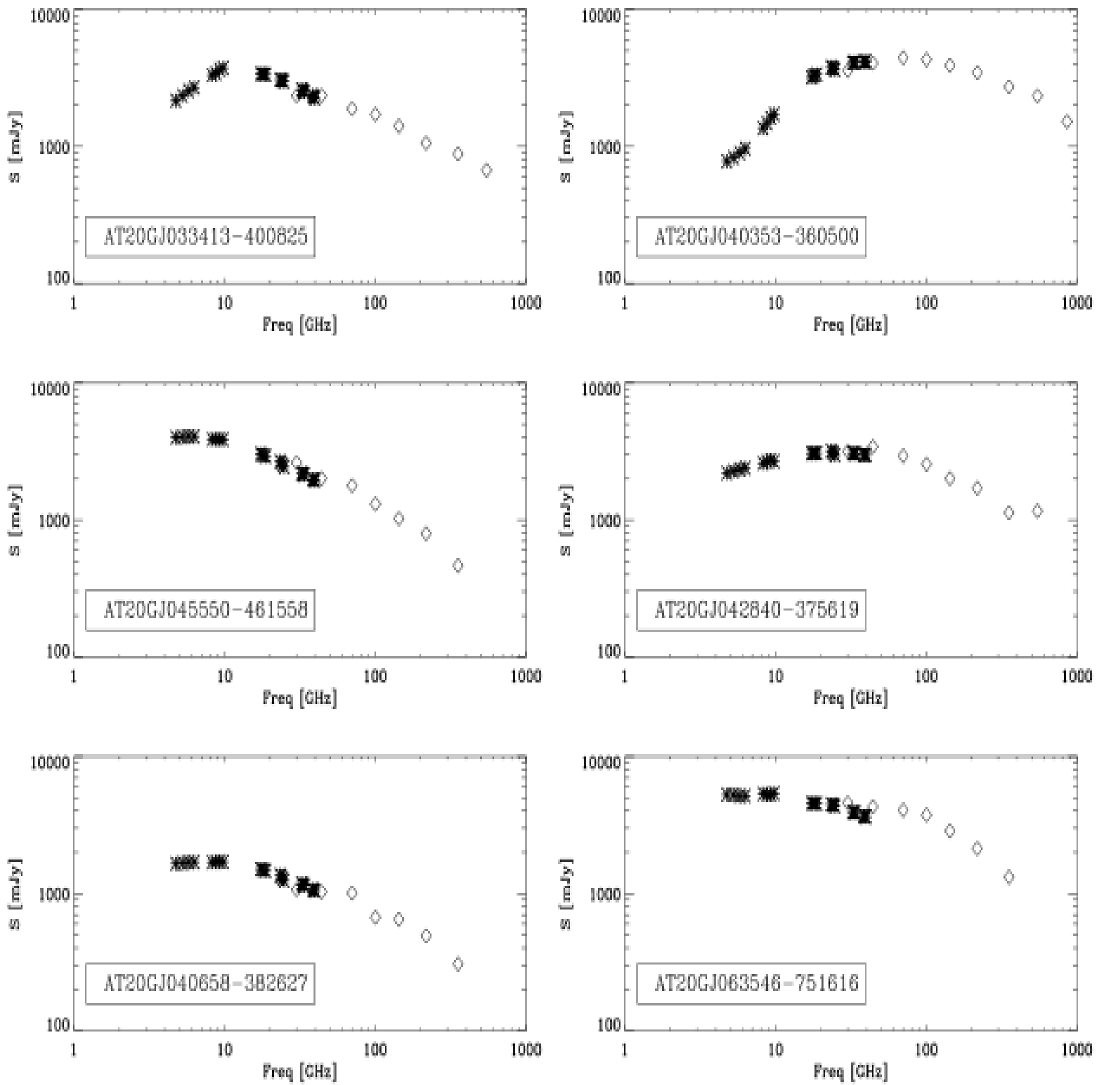

Type	$200 \leq S_{20\,\mathrm{GHz}} < 500$ mJy (per cent)	$S_{20\,\mathrm{GHz}} \geq 500$ mJy (per cent)
Flat	5.1	10.3
Steep	13.3	3.6
Inverted	0	0.6
Peaked	11.2	14.5
Downturning	65.3	66
Self-absorbed	5.1	4.8
Upturning	0	0

(Bonavera et al. 2012)

Synchrotron in AGN

As more energetic photons are also less absorbed (i.e. electron clouds are less thick) the inner and denser regions of the AGN become less optically thick and become more easily observable as the frequency of observation increases.

Hence, mm observations of AGN provide information on the jet structure and unveil the details of their basis getting closer to the black hole.

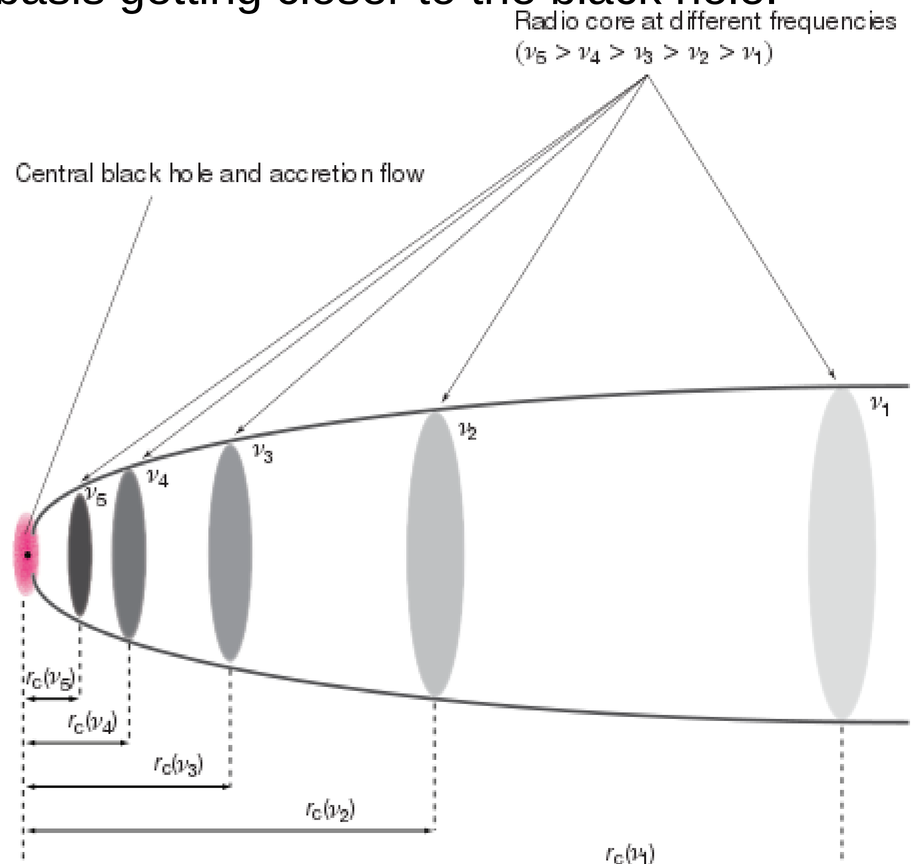

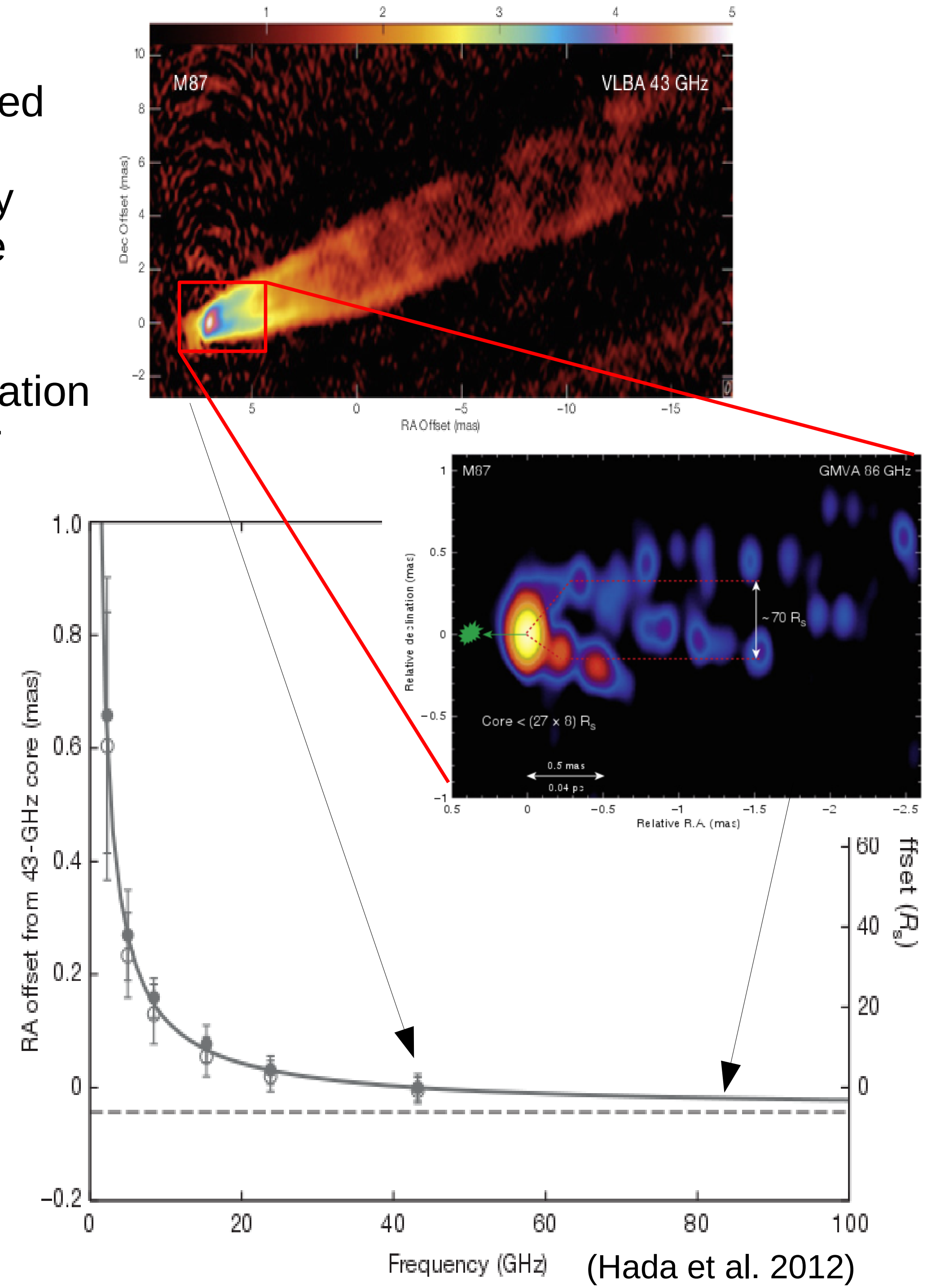

(Hada et al. 2012)

Dust

Dust grains are solid, macroscopic particles composed of dielectric and refractory materials (mostly silicates or graphites). Typical grain sizes in interstellar dust ranges between few nm to few microns.

In our Galaxy the gas-to-dust ratio is about 100:1.
(ISM is about 10% of the baryonic mass of the Galaxy -> dust is roughly 0.1% of the total)

What is the role of dust?
- they scatter star light modifying the signals
- they absorb roughly 30-50% of the starlight emitted by the Galaxy
- re-radiate it as far-infrared continuum emission
  (1/3-1/2 of the bolometric luminosity of the Galaxy!)
- are the primary sites of molecular formation, and play the catalyst role
  (all of the H2 in the ISM form on grains).

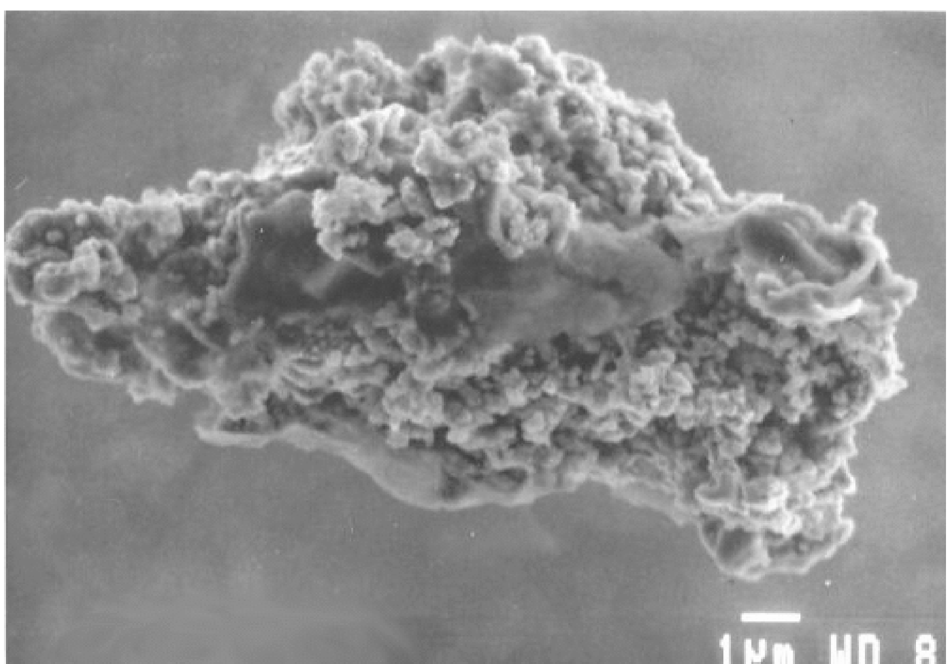

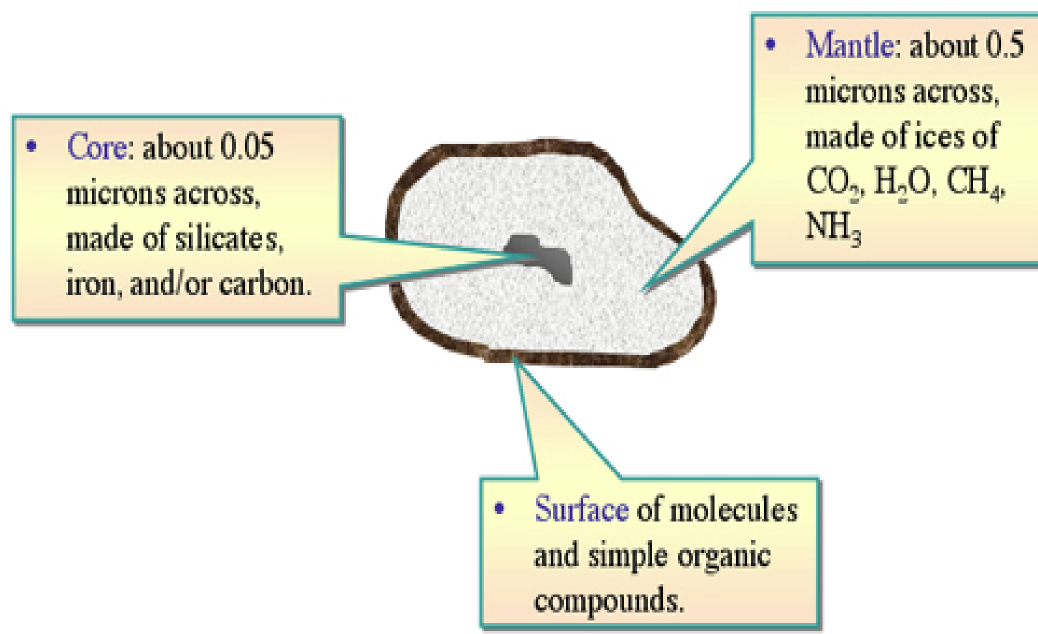

Dust scattering

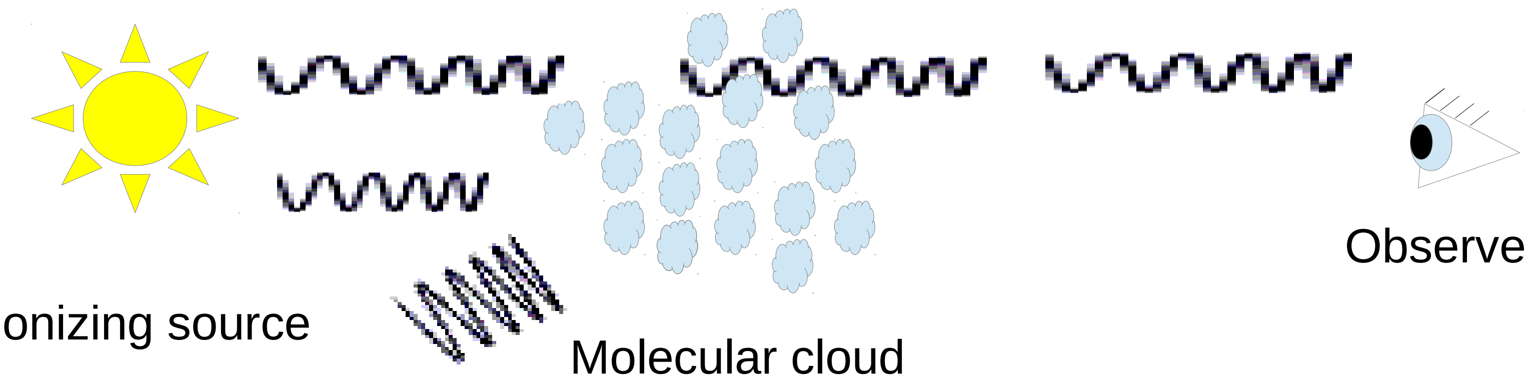

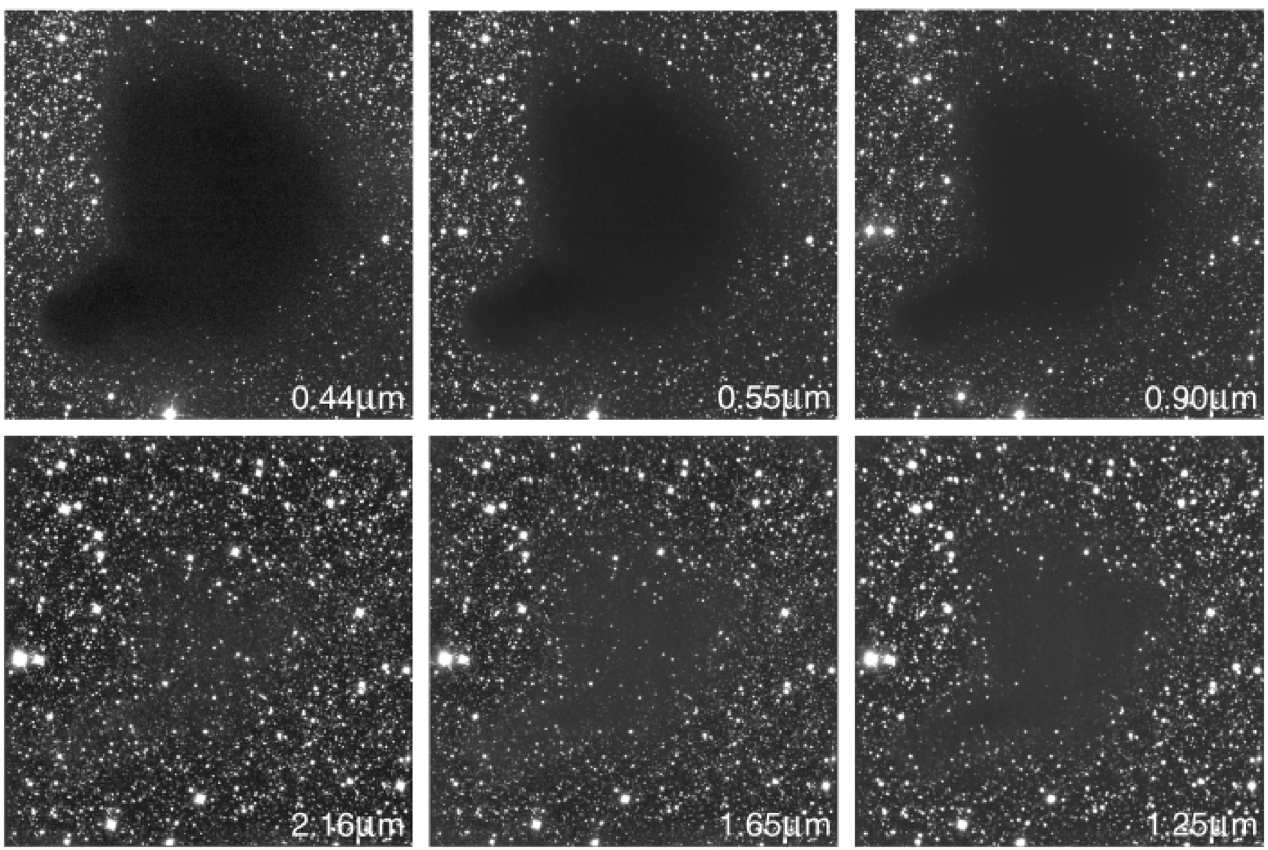

The Dark Cloud B68 at Different Wavelengths (NTT + SOFI)

Our view is blocked in visible light because the dust grains are about the same size as optical wavelengths - about one micron or less - and so are very effective at scattering or absorbing that light.
But longer infrared wavelengths undulate around the dust.
The longer the wavelength, the thicker the layer of dust it can penetrate.
So sub(mm) radiation can move freely through the Universe, unobstructed by dust.

Dust emission

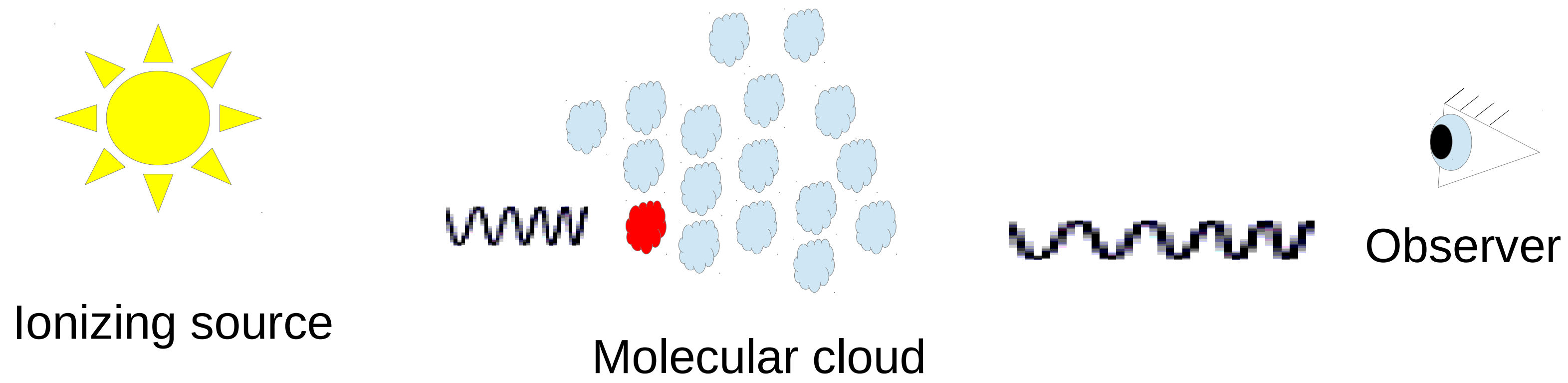

Graphite and silicate dust grains absorb opt-UV radiation and heats up (photoionization).

The visible and ultraviolet light that the dust absorbs warms the grains just enough for them to re-radiate the light at sub(mm) wavelengths. The colder the grains, the longer the wavelength of emission.

Evolved stars (e.g. ages above 100–200Myr) contribute significantly to the dust heating, which tends to cause the IR luminosity to overestimate the SFR. The fraction of dust heating from young stars varies by a large factor among galaxies; **in extreme circumnuclear starburst galaxies or individual star-forming regions, nearly all of the dust heating arises from young stars, in evolved galaxies with low specific SFRs, the fraction can be as low as~10%.**

Dust grains show linear polarization, which leads to the conclusion that grains are elongated and aligned by magnetic fields. The direction but not the strength of the magnetic field can be determined from dust polarization. The fractional polarization is rather small, so requires high sensitivity and care to keep instrumental effects small

Dust emission

The equation of transfer is

$$\frac{\mathrm{d}I_\nu}{\mathrm{d}s} = -\kappa_\nu I_\nu + \varepsilon_\nu$$

linear absorption coefficient κ_ν

emissivity ε_ν

In TE a black body brightness is described by a Planckian

$$B_\nu(T) = \frac{2h\nu^3}{c^2}\frac{1}{\mathrm{e}^{h\nu/kT} - 1}$$

Defined the **optical depth** as

$$\mathrm{d}\tau_\nu = -\kappa_\nu \, \mathrm{d}s$$

We get

$$-\frac{1}{\kappa_\nu}\frac{\mathrm{d}I_\nu}{\mathrm{d}s} = \frac{\mathrm{d}I_\nu}{\mathrm{d}\tau_\nu} = I_\nu - B_\nu(T)$$

That solves in

$$I_\nu(s) = I_\nu(0)\,\mathrm{e}^{-\tau_\nu(s)} + \int_0^{\tau_\nu(s)} B_\nu(T(\tau))\,\mathrm{e}^{-\tau}\,\mathrm{d}\tau$$

For isothermal medium

$$I_\nu(s) = I_\nu(0)\,\mathrm{e}^{-\tau_\nu(s)} + B_\nu(T)\,(1 - \mathrm{e}^{-\tau_\nu(s)})$$

$T(\tau) = T(s) = T = \mathrm{const}$

For optically thick medium

$\tau_\nu(0) \to \infty$ $\qquad$ $I_\nu = B_\nu(T)$

The difference
is an on-source minus off-source
measurement

$$\Delta I_\nu(s) = I_\nu(s) - I_\nu(0) = (B_\nu(T) - I_\nu(0))(1 - \mathrm{e}^{-\tau})$$

Dust emission

For an isothermal absorber
(i.e. no background source)

$$I_\nu = B_\nu(T)\,(1 - \mathrm{e}^{-\tau_\nu})$$

that can be rewritten in RJ regime as
where T_{dust}>>T_0=hν/k

$$T_{\mathrm{dust}} = T_0 \left(\frac{1}{\exp\{T_0/T_{\mathrm{dust}}\} - 1}\right)(1 - \mathrm{e}^{-\tau_{\mathrm{dust}}})$$

Absorption coefficient depends on grain shape and distribution and for lambda>0.1mm
The usual relation is

$$\tau_{\mathrm{dust}} = 7 \times 10^{-21}\,\frac{Z}{Z_\odot}\,b\,N_{\mathrm{H}}\,\lambda^{-2}$$

where N_H is the H column density (in all the forms),
Z the metallicity, and b=1.9 for moderate density and b=3.4 for dense gas but it is adjustable to account for the grain size.

If optical depth is small (like in mm band)

$$T = T_{\mathrm{dust}}\,\tau_{\mathrm{dust}}$$

Then the **flux is**

$$S = \frac{2\,k\,T}{\lambda^2} = 2\,k\,T_{\mathrm{dust}}\lambda^{-2}\,\tau_{\mathrm{dust}}\Delta\Omega$$

The relation between dust flux and column density is (source clumping introduces further uncertainties)

$$N_{\mathrm{H}} = 1.93 \times 10^{24}\,\frac{S_\nu}{\theta^2}\,\frac{\lambda^4}{Z/Z_\odot\,b\,T_{\mathrm{dust}}}$$

The dust optical depth is small and goes as $\lambda^{-\beta}$ with $1<\beta<2$ so that the flux density goes as λ^{-3} to λ^{-4}.

Dust emission spectra

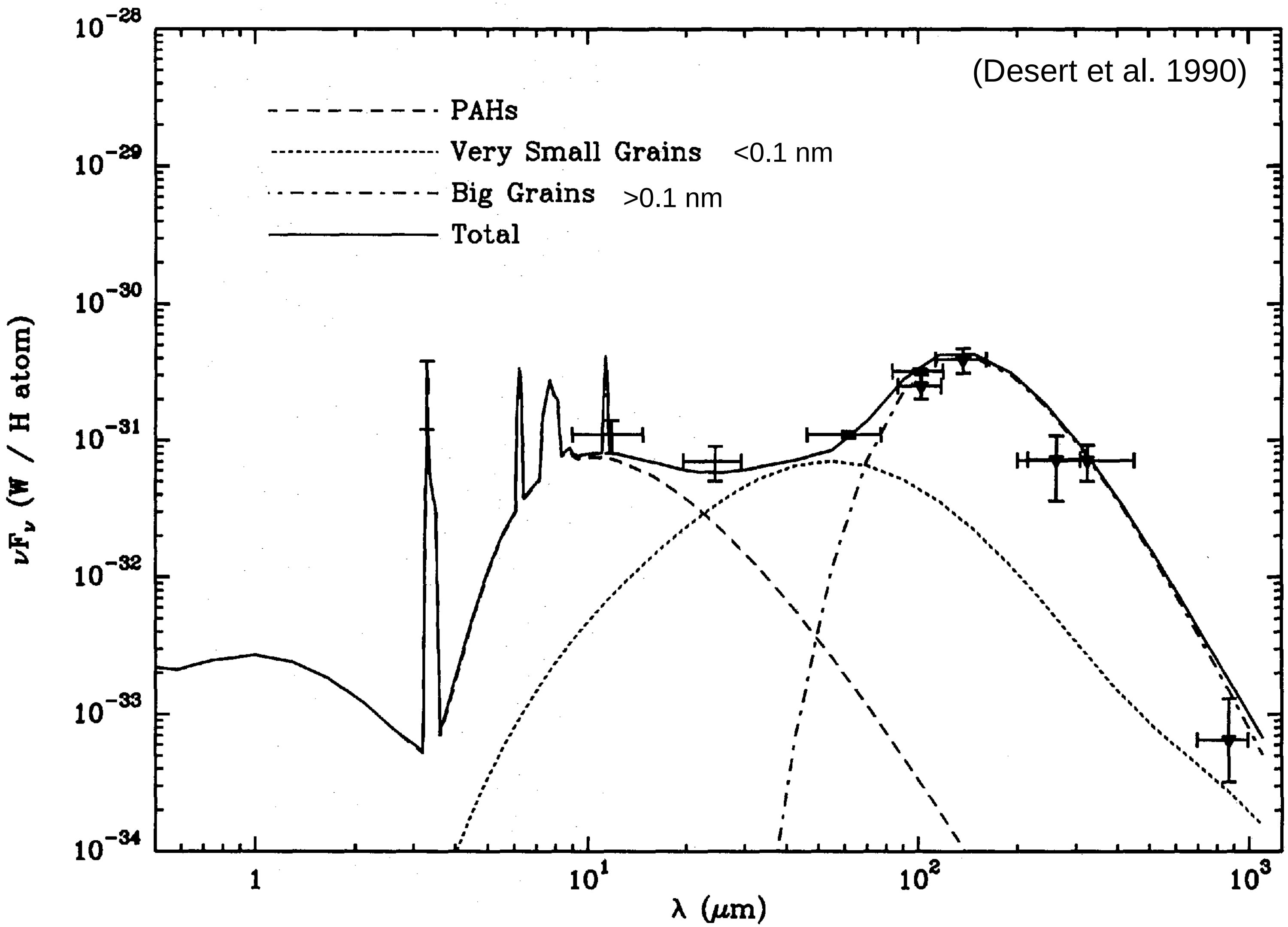

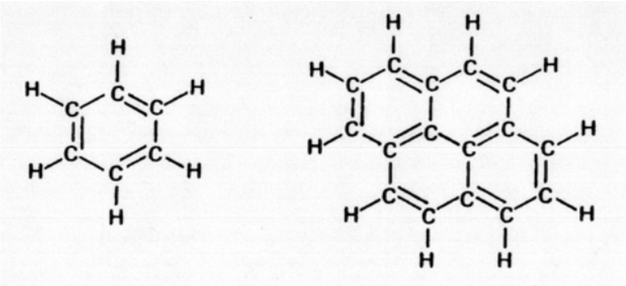

Polycyclic Aromatic Hydrocarbons
are combinations of aromatic rings
(e.g. benzene)

Info from the dust profiles

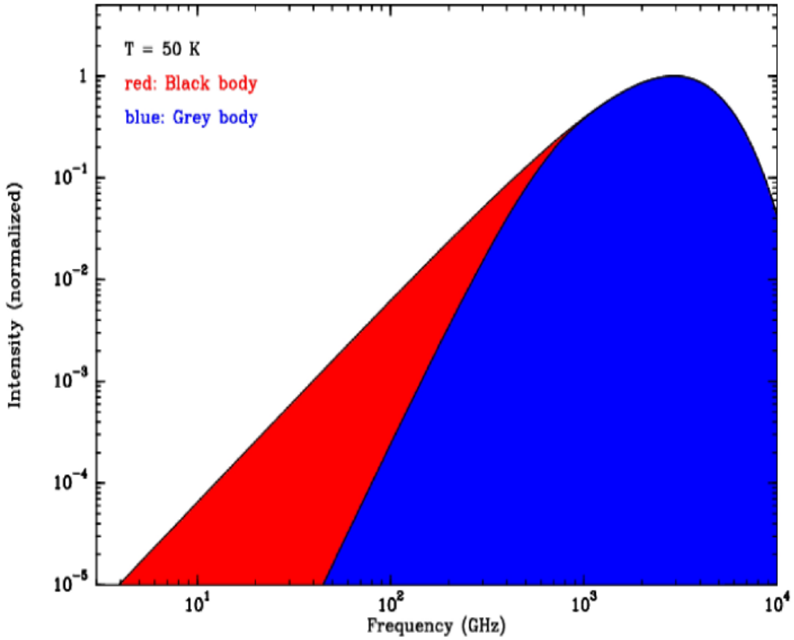

Temperature By fitting a greybody spectrum

$$T = T_{\rm dust}\,\tau_{\rm dust}$$

it is possible to estimate the temperature. Assumptions have to be done on the dust grain properties

Mass Given the temperature, mass is

$$M_{\rm d} = \frac{D_{\rm L}^2 S_{\nu_{obs}}}{(1+z)\kappa_\nu B_\nu(T_{\rm d})} \qquad k_\nu \propto \nu^\beta$$

depending on the grain properties through the absorption coefficient (0.04-0.15 m2/kg at 1mm)

Photometric redshifts can be retrieved via SED fitting with template models. A degeneracy remains with temperature

(Sub)mm measurements are crucial to reconstruct the dust peak and improve the SED fitting qualities. Issues can be added by the presence of AGNs

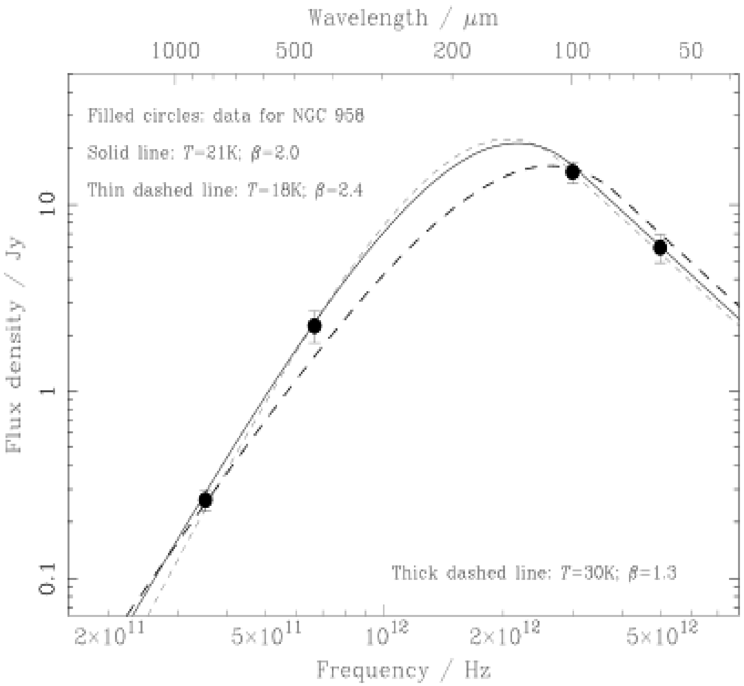

The negative k correction

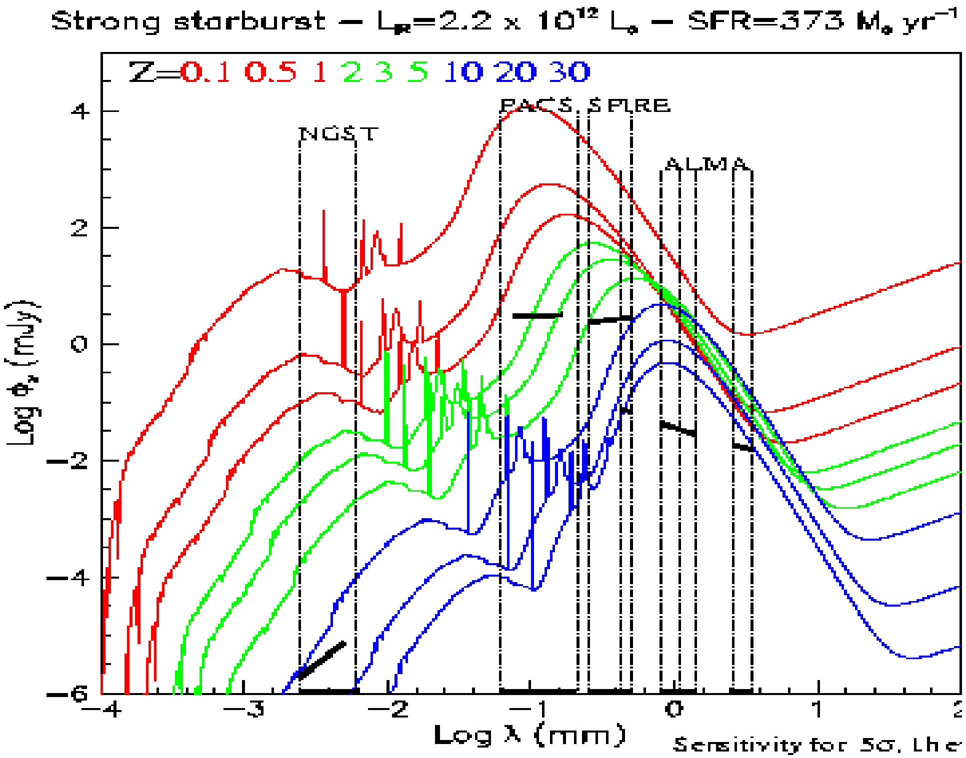

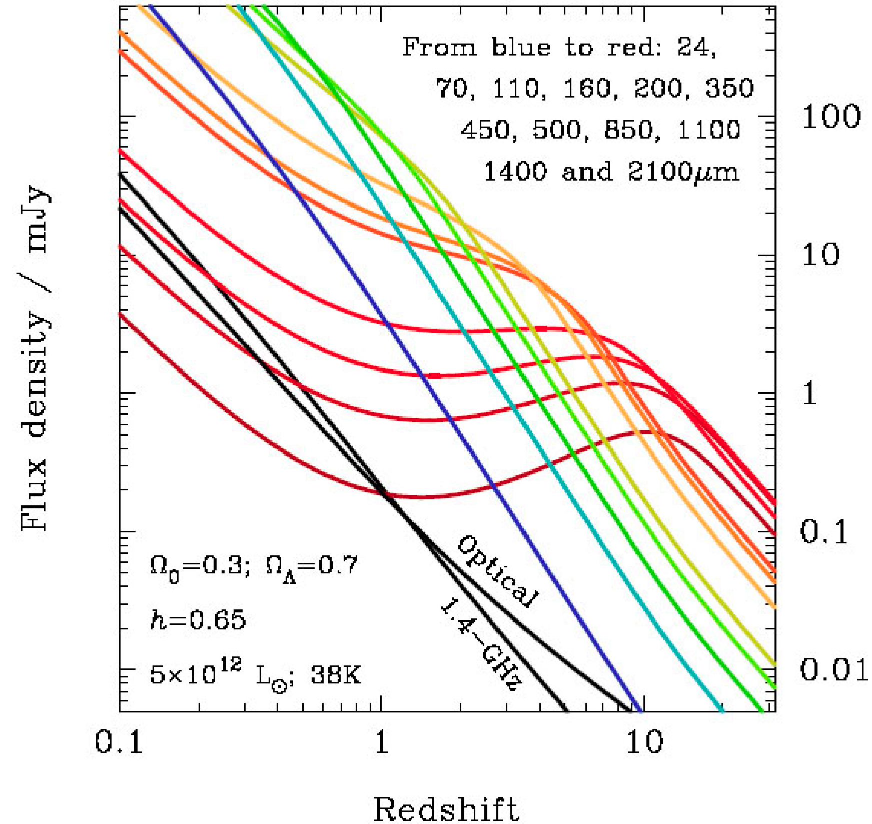

Given the dust scaling with frequency, the net effect of redshifting dust spectra is that to more than compensate the inverse square law of decreasing flux density with z
In the mm band the same dusty galaxy appear brighter at increasing redshift.
Deep mm band fields are dominated by high-z galaxies

(Blain et al. 1993, 2002)

Line transitions

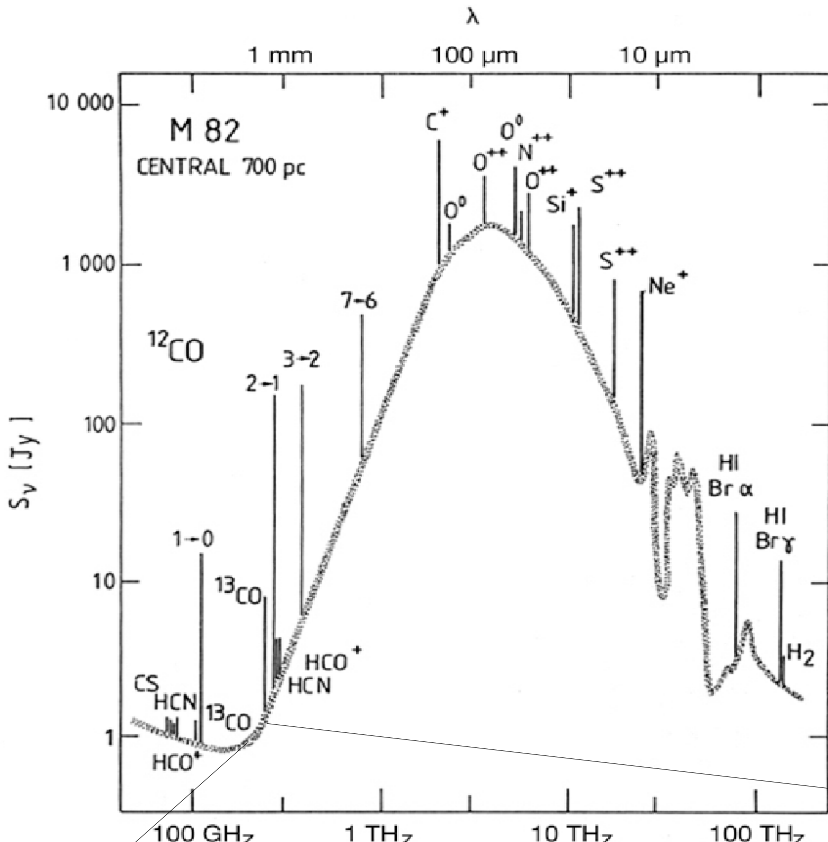

- Continuum is dominated by dust and synchrotron

- Spectra show a very rich chemistry

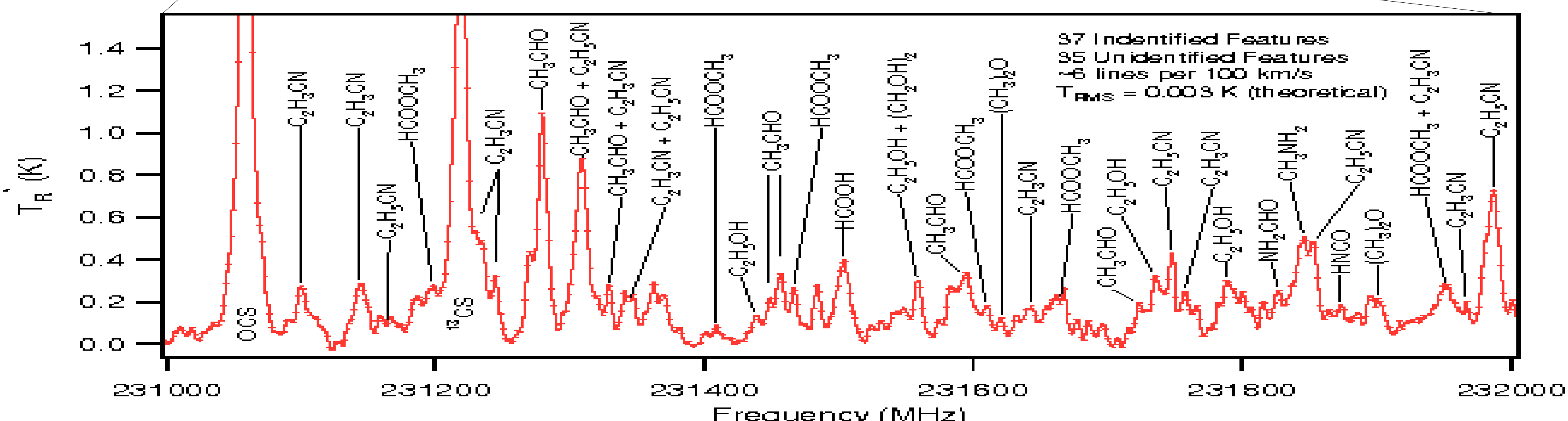

Molecular lines

Molecular transitions according to different energies, W :

a) electronic transitions with typical energies of a few eV – that is lines in the visual or UV regions of the spectrum;

b) vibrational transitions caused by oscillations of the relative positions of nuclei with respect to their equilibrium positions. Typical energies are 0. 1− 0. 01 eV, corresponding to lines in the infrared region of the spectrum;

c) **rotational transitions caused by the rotation of the nuclei with typical energies of ∼= 10−3 eV corresponding to lines in the cm and mm wavelength range.**

$$W^{\mathrm{tot}} = W^{\mathrm{el}} + W^{\mathrm{vib}} + W^{\mathrm{rot}}$$

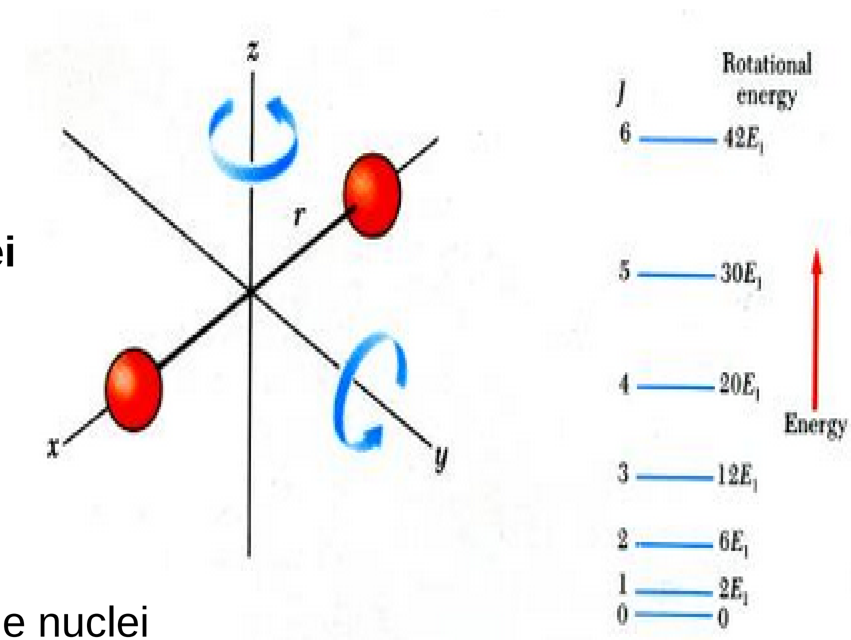

J is the molecular orbital angular momentum number corresponding to the angular momentum perpendicular to the line connecting the nuclei

$$L = I\omega = \left(\frac{m_A m_B}{m_A + m_B}\right) r_e^2 \omega = m r_e^2 \omega \qquad E_{\mathrm{rot}} = \frac{I\omega^2}{2} = \frac{L^2}{2I} = \frac{J(J+1)\hbar^2}{2I}$$

the quantum of energy associated with a transition from J to J-1 is

$$\Delta E_{\mathrm{rot}} = [J(J+1) - (J-1)J]\frac{\hbar^2}{2I} = \frac{\hbar^2 J}{I}$$

(I is the inertia momentum). That corresponds to a ladder at frequencies

$$\nu = \frac{\Delta E_{\mathrm{rot}}}{h} = \frac{\hbar J}{2\pi I} = \frac{hJ}{4\pi^2 m r_e^2}\,, \qquad J = 1,\ 2, \ldots$$

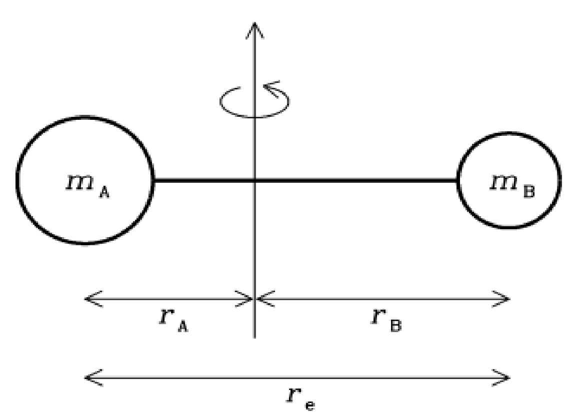

Atomic lines

Atomic transitions at sub(mm) wavelengths mostly arise from spin-orbit interactions: by changing the spin direction, the electron jumps from a fine structure level to another, because of an electromagnetic interaction between the electron's spin and the magnetic field generated by the electron's orbit around the nucleus.

In molecular clouds such transitions can be collisionally stimulated.

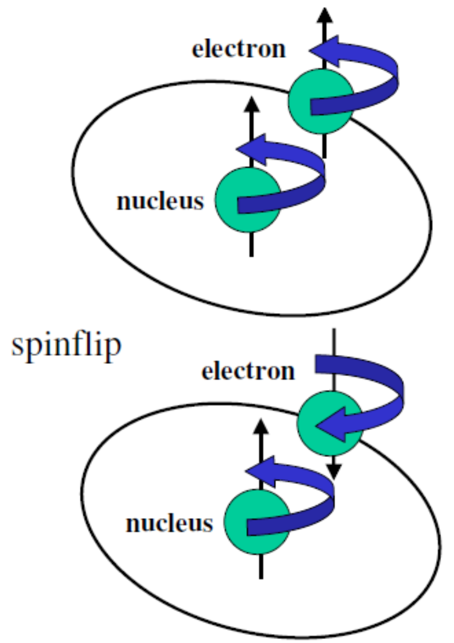

J is the total angular momentum number so that J=L±S with L=0,...,n-1

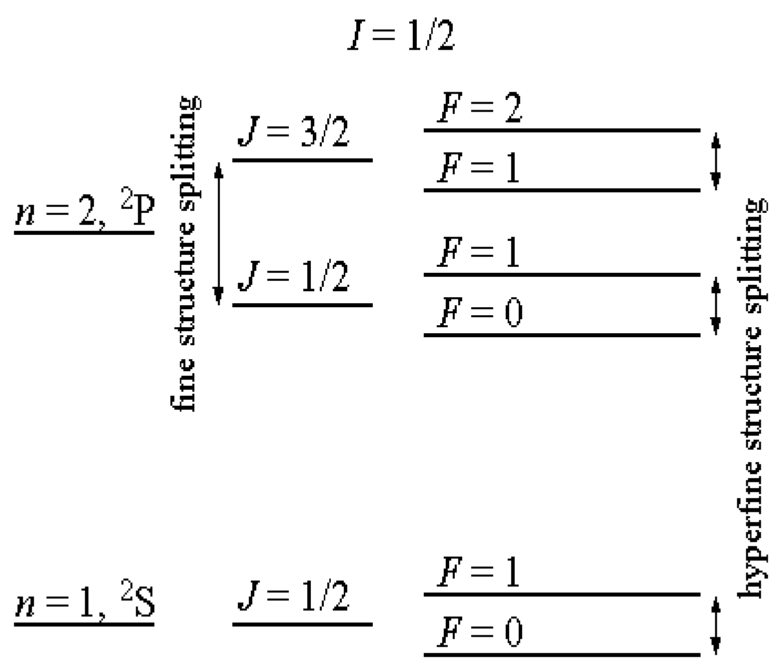

Line transitions

Transitions probability per unit time between different energetic levels can be expressed through Einstein coefficients:

A_{21} for spontaneous emission
$B_{21}U$ for induced emission (radiation)
$B_{12}U$ for absorption (radiation)

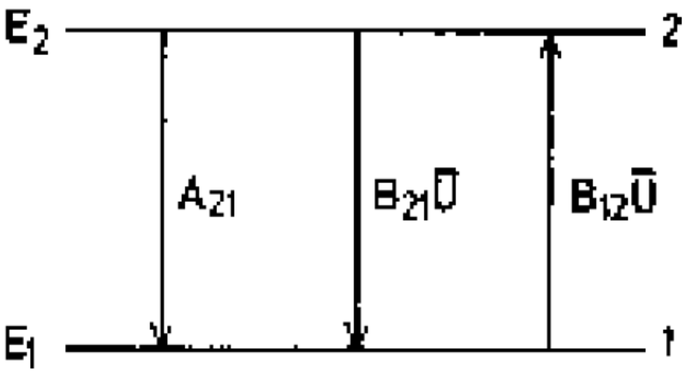

At equilibrium considering only radiation field

$$n_1 B_{12} U(T) = n_2 (A_{21} + B_{21} U(T))$$

Solving in U

$$U(T) = \frac{A_{21}}{\frac{n_1}{n_2} B_{12} - B_{21}}$$

the average energy density per radiation field and B is a Planckian in LTE

$$U(T) = \frac{4\pi}{c} B(T_b) = \frac{8\pi\nu^3}{c^3} \frac{1}{e^{h\nu/kT} - 1}$$

This is correct only if

$$\frac{A_{21}}{B_{21}} = \frac{8\pi h\nu^3}{c^3} \qquad \frac{B_{21}}{B_{12}} = \frac{g_1}{g_2}$$

Boltzmann distribution in the levels

$$\frac{n_2}{n_1} = \frac{g_2}{g_1} e^{-h\nu/k_B T}$$

Line transitions

The energy for the different transitions is:

-for spontaneous emission

$$\mathrm{d}E_{\mathrm{e}}(\nu) = h\nu_0\, N_2\, A_{21}\, \varphi_{\mathrm{e}}(\nu)\, \mathrm{d}V \frac{\mathrm{d}\Omega}{4\pi}\, \mathrm{d}\nu\, \mathrm{d}t$$

$$\mathrm{d}E_{\mathrm{a}}(\nu) = h\nu_0\, N_1\, B_{12} \frac{4\pi}{c}\, I_\nu\, \varphi_{\mathrm{a}}(\nu)\, \mathrm{d}V \frac{\mathrm{d}\Omega}{4\pi}\, \mathrm{d}\nu\, \mathrm{d}t$$

-for induced emission

$$\mathrm{d}E_{\mathrm{s}}(\nu) = h\nu_0\, N_2\, B_{21} \frac{4\pi}{c}\, I_\nu\, \varphi_{\mathrm{e}}(\nu)\, \mathrm{d}V \frac{\mathrm{d}\Omega}{4\pi}\, \mathrm{d}\nu\, \mathrm{d}t$$

-for absorption

The total power is

$$\mathrm{d}E_{\mathrm{e}}(\nu) + \mathrm{d}E_{\mathrm{s}}(\nu) - \mathrm{d}E_{\mathrm{a}}(\nu) = \mathrm{d}I_\nu\, \mathrm{d}\Omega\, \mathrm{d}\sigma\, \mathrm{d}\nu\, \mathrm{d}t$$

That solves in the equation of transfer with Einstein coefficients

$$\frac{\mathrm{d}I_\nu}{\mathrm{d}s} = -\frac{h\nu_0}{c}\,(N_1\, B_{12} - N_2\, B_{21})\, I_\nu\, \varphi(\nu) + \frac{h\nu_0}{4\pi} N_2\, A_{21}\, \varphi(\nu)$$

$$\frac{\mathrm{d}I_\nu}{\mathrm{d}s} = -\kappa_\nu I_\nu + \varepsilon_\nu$$

$$\frac{\varepsilon_\nu}{\kappa_\nu} = B_\nu(T)$$

$$\frac{n_2}{n_1} = \frac{g_2}{g_1} e^{-h\nu/k_{\mathrm{B}}T}$$

Line transitions

Transitions probability per unit time between different energetic levels can be expressed through Einstein coefficients:

A_{21} for spontaneous emission
$B_{21}U$ for induced emission (radiation)
γ_{21} for induced emission (collisions)
$B_{12}U$ for absorption (radiation)
γ_{12} for absorption (collisions)

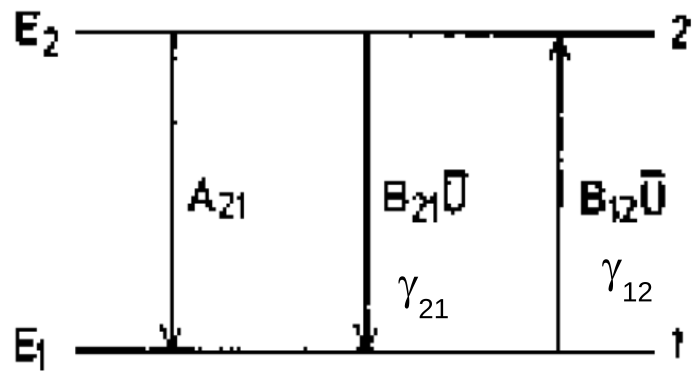

At equilibrium

$$n_1(\gamma_{12}+B_{12}U(T))=n_2(A_{21}+\gamma_{21}+B_{21}U(T))$$

The collision rate is given by
(density times collision probability per particle(velocity distribution))

$$C_{ik}=n\,\gamma_{ik}(v)$$

$$\frac{C_{12}}{C_{21}}=\frac{n_2\gamma_{21}}{n_1\gamma_{12}}=\frac{g_2}{g_1}\,e^{-h\nu/kT_K}$$

While the energy density due to the radiation field is

$$U(T)=\frac{4\pi}{c}B(T_b)=\frac{8\pi\nu^3}{c^3}\frac{1}{e^{h\nu/kT_b}-1}$$

Spectral lines

$$\frac{n_2 g_1}{n_1 g_2}=\exp\left(\frac{-h\nu}{kT_{ex}}\right)=\exp\left(\frac{-h\nu}{kT_b}\right)\frac{A_{21}+C_{21}\exp\left(\frac{-h\nu}{kT_K}\right)\left[\exp\left(\frac{h\nu}{kT_b}\right)-1\right]}{A_{21}+C_{21}\left[1-\exp\left(\frac{-h\nu}{kT_b}\right)\right]}$$

$$T_{ex},T_b,T_K\gg T_0=\frac{h\nu}{k}$$

$$T_{ex}=T_K\frac{T_b A_{21}+T_0 C_{21}}{T_K A_{21}+T_0 C_{21}}$$

If radiation dominates (low density) C_{21}<<A_{21} then T_{ex}-> T_b and no line is observable
If collisions dominate (high density) C_{21}>>A_{21} then T_{ex}-> T_K and line is observable

The critical density is the density of the cloud at which the probability of emission equals the probability of collisional processes

$$n_{cr}\approx A_{21}\approx C_{21}$$

Observations in a given transition are most sensitive to gas with densities near the corresponding critical density.

Given the on-off source Measurement

$$\Delta I_\nu=I_\nu(T_K)-B_\nu(T_b)=(1-e^{-\tau})\frac{2h\nu^3}{c^2}\left(\frac{1}{e^{h\nu/kT_K}-1}-\frac{1}{e^{h\nu/kT_b}-1}\right)$$

If Tk > Tb the line appears in emission
If Tk < Tb the line appears in absorption

Spectral lines position and broadening

Spectral lines are Doppler shifted if emitting cloud is moving wrt the observer.

$$1+z=\frac{\nu_{emitted}}{\nu_{observed}}$$

Variation in the line position wrt the rest frame is a measure of cosmological distances.

Spectral lines can be broadened for

$$\frac{\Delta v}{c}=\frac{\Delta \nu}{\nu}$$

- **natural broadening**: According to the uncertainty principle the uncertainty in energy, ΔE and the lifetime, Δt, of the excited state are related by ΔE/Δt>h/2 This determines the minimum possible line width.

- **Doppler broadening**: due to intrinsic motions of (parts of) the cloud wrt the observer The higher the temperature of the cloud, the wider the distribution of velocities in the cloud Hence the emission is characterized by a velocity distributions that is described by the shape of the spectral lines with frequency A(ν). If this were the only effect the line shape would be Gaussian

- **Pressure broadening** (Collision broadening). Collisions between atoms or molecules reduce the lifetime of the upper state, Δt, increasing the uncertainty ΔE.

Spectral lines shape

The line shape is a function of the frequency and hence of the velocity A(ν)

$$M_0 = \Delta v \sum_v A(v)$$

The **zeroth momentum** of the distribution is the integrated flux density

The **first momentum** of the distribution is the intensity-weighted velocity of the spectral line and hence a measure for the mean velocity of the gas.

$$M_1 = \frac{\sum_v v\,A(v)}{\sum_v A(v)}$$

The **second momentum** is a measure for the velocity dispersion, σ, of the gas along the line of sight, i.e. the width of the spectral line

$$M_2 = \sqrt{\frac{\sum_v (v - M_1)^2 A(v)}{\sum_v A(v)}}$$

By mapping the sources in different frequency channels, allows to reconstruct the spatial distribution of the velocity field

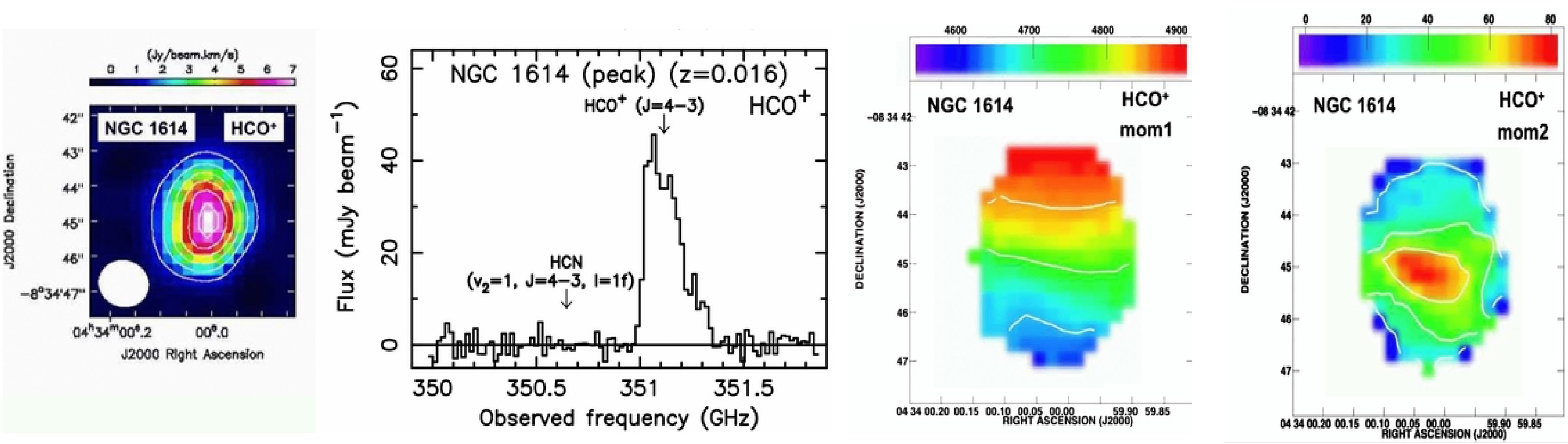

(ALMA HCO+ In NGC 1614
Imanishi et al. 2013)

Line signatures

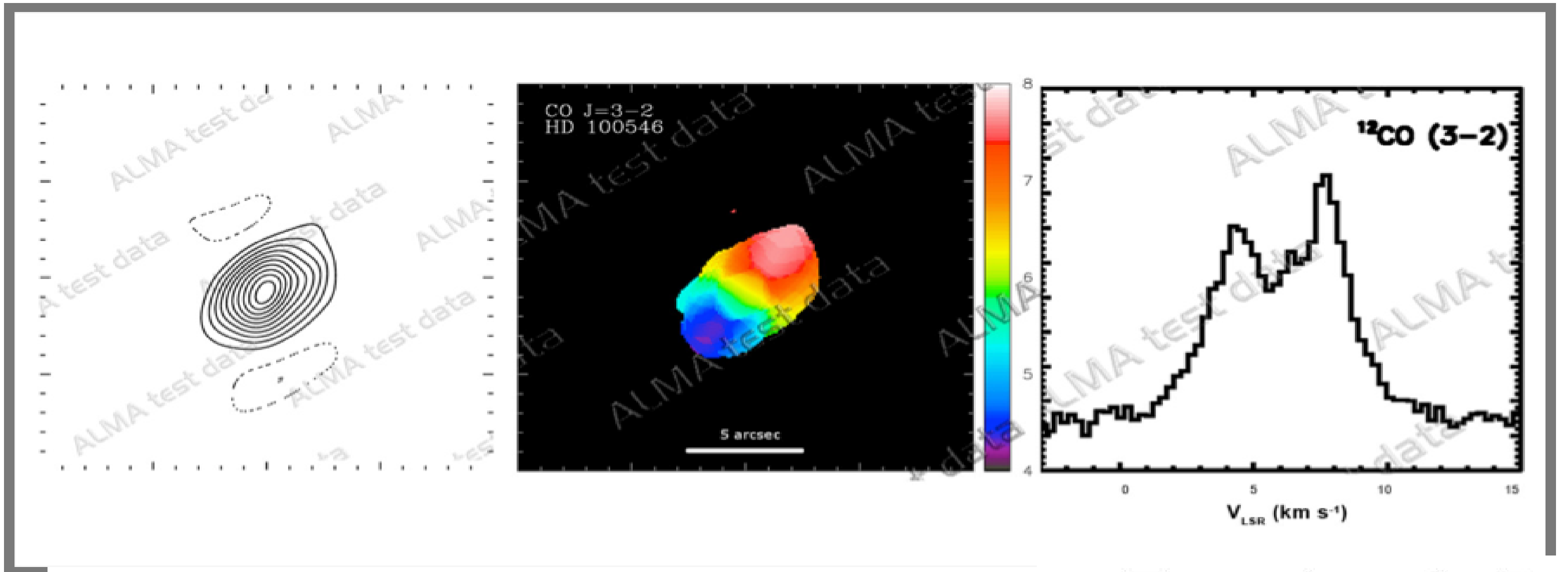

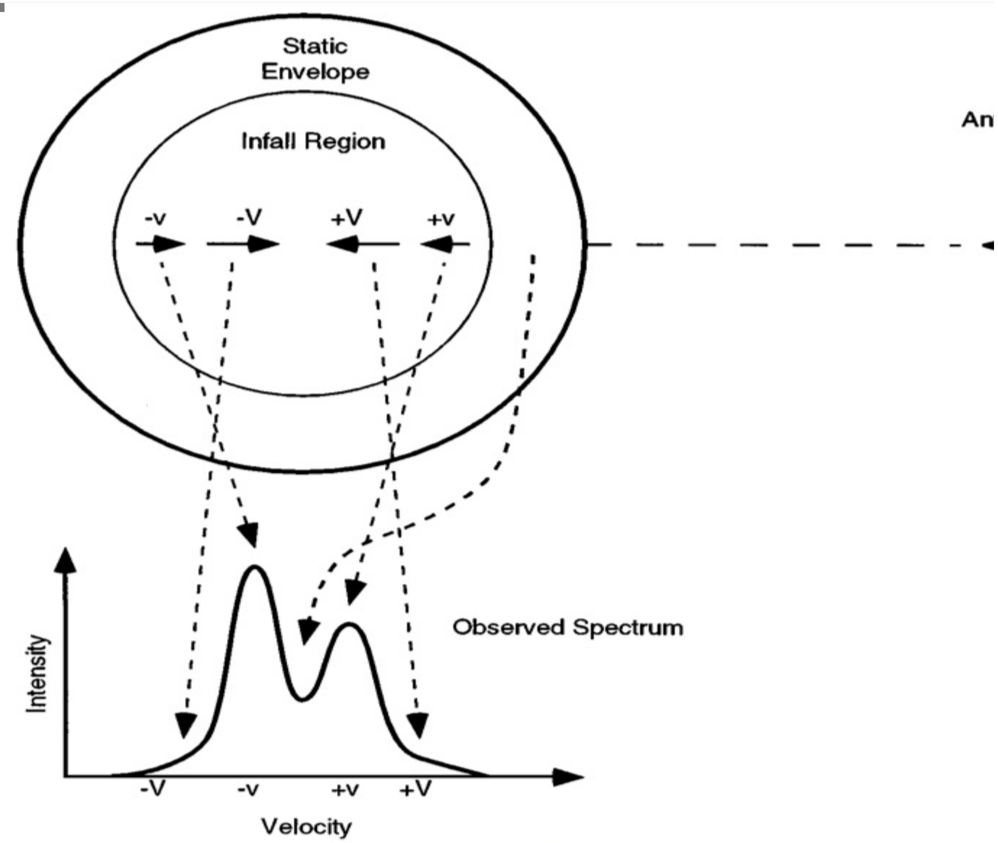

Formation of a P-Cygni Line- Profile

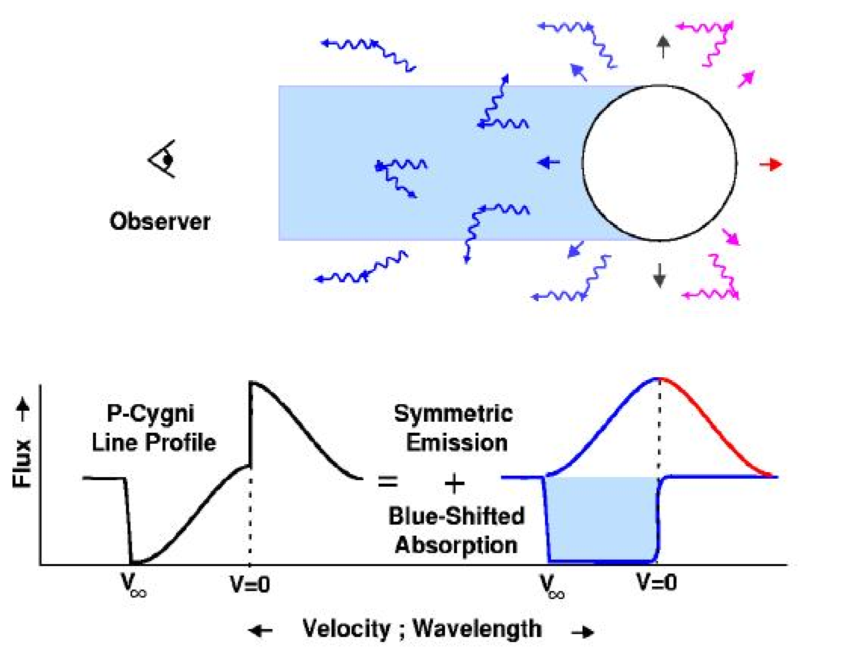

PDRs

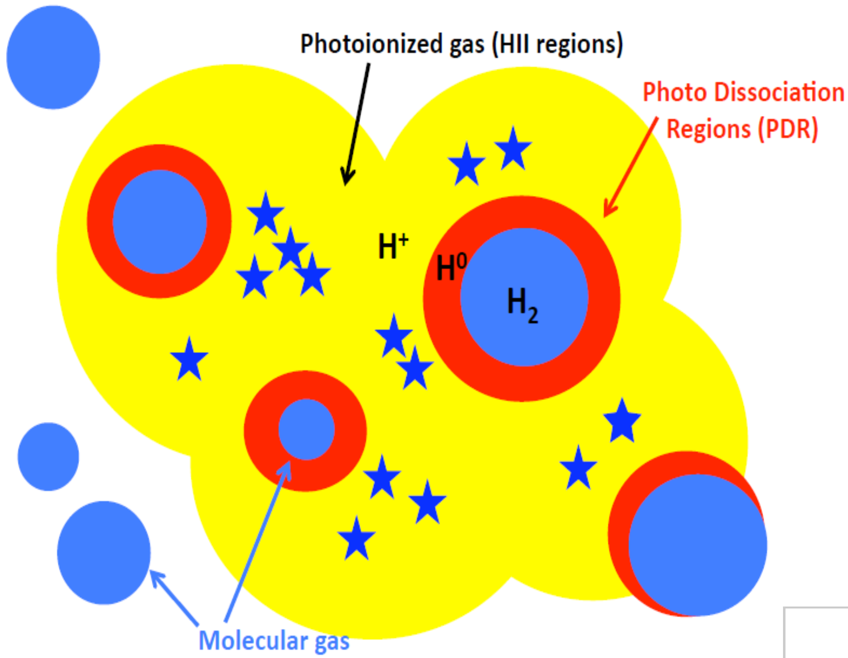

Photo-Dissociation Regions (PDR=photon-dominated regions) are the warm, partially ionized surfaces between the region where UV radiation from stars ionizes the gas and the cold molecular clouds. In these regions H2 is dissociated in HI. These regions are also rich of dust. Excitation From UV radiation together with low density make PDR the origin of spectral lines in FIR and sub-mm

The dominant species are H, C, O and N.

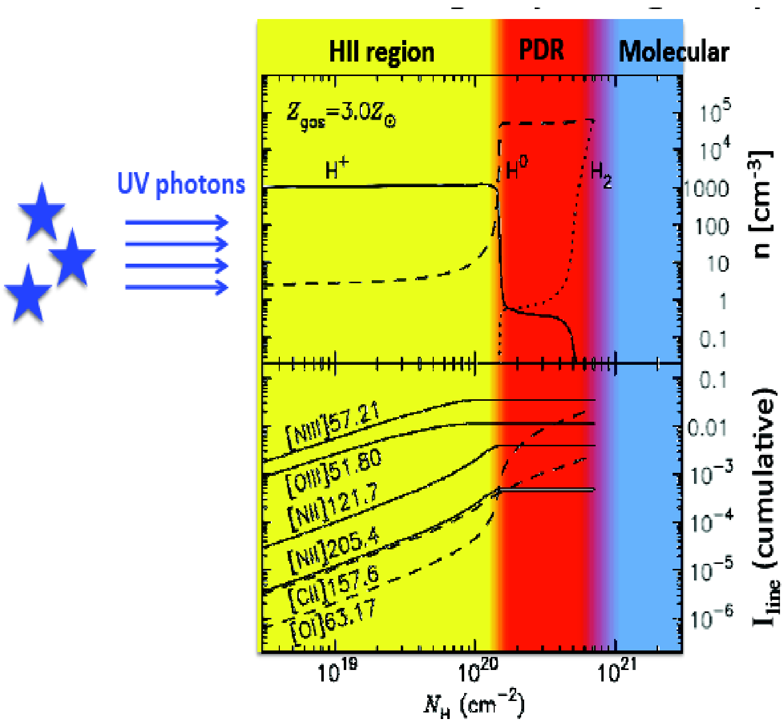

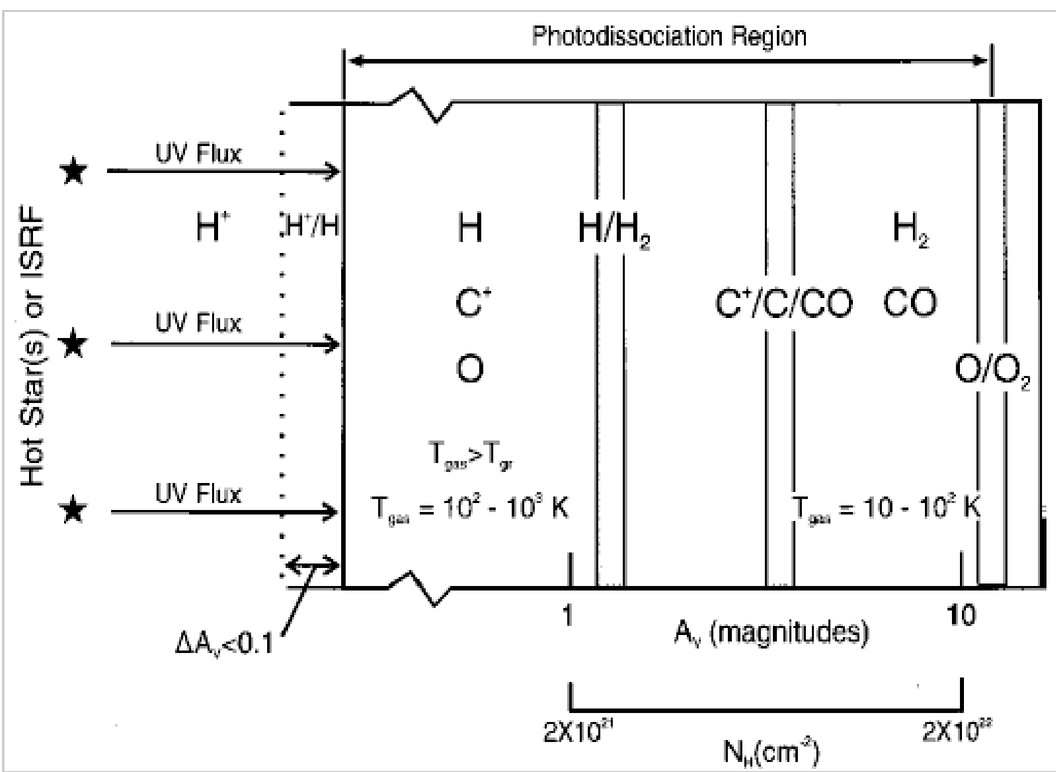

Atomic lines

Element and ionization state	Transition	ν/GHz	A_{ij}/s^{-1}	Critical density n^*	Notes
CI	${}^3P_1 - {}^3P_0$	492.16	7.93×10^{-8}	5×10^2	b
CI	${}^3P_2 - {}^3P_1$	809.34	2.65×10^{-7}	10^4	b
CII	${}^2P_{3/2} - {}^2P_{1/2}$	1900.54	2.4×10^{-6}	5×10^3	b
OI	${}^3P_0 - {}^3P_1$	2060.07	1.7×10^{-5}	$\sim 4 \times 10^5$	b
OI	${}^3P_1 - {}^3P_2$	4744.77	8.95×10^{-5}	$\sim 3 \times 10^6$	a,b
OIII	${}^3P_1 - {}^3P_0$	3392.66	2.6×10^{-5}	$\sim 5 \times 10^2$	a
OIII	${}^3P_2 - {}^3P_1$	5785.82	9.8×10^{-5}	$\sim 4 \times 10^3$	a
NII	${}^3P_1 - {}^3P_0$	1473.2	2.1×10^{-6}	$\sim 5 \times 10^1$	a
NII	${}^3P_2 - {}^3P_1$	2459.4	7.5×10^{-6}	$\sim 3 \times 10^2$	a
NIII	${}^2P_{3/2} - {}^2P_{1/2}$	5230.43	4.8×10^{-5}	$\sim 3 \times 10^3$	a,b

[a] ions or electrons as collision partners
[b] H_2 as a collision partner

In cold regions, cooling is dominated by collisional excitation of C+
by collisions with thermal electrons followed by emission of infrared fine-structure lines.
As the temperature rises, other species begin to contribute collisionally excited lines to the cooling

CII

The ground state of C+ has a fine-structure transition with excitation energy (in temperature units) of 92 K, which emits a far-infrared photon with a wavelength of 158μm.

The [CII] line traces photodissociation regions (PDRs) as well as diffuse HI and HII regions. It should be an excellent tracer of the global galactic star formation activity, including that of somewhat lower-mass (A+B) stars (Stacey et al 1991).

The line emission contains between 0.1 and 1% of the bolometric luminosity of any galaxy.

In local galaxies, the [CII] line is proportional to total far-IR flux.
-3<log(L_CII/Lfir)<-2 in local LIRG.
The ratio drops by a factor 10 in ULIRGs (because of stronger UV fields, higher opacity, or presence of AGN).
The ratio is an order of magnitude higher at higher z for objects of the same luminosity (lower dust content = lower metallicities and more efficient cooling, Maiolino et al. 2009).
There is a trend for AGNs to have lower L_CII/Lfir ratios than SMGs.

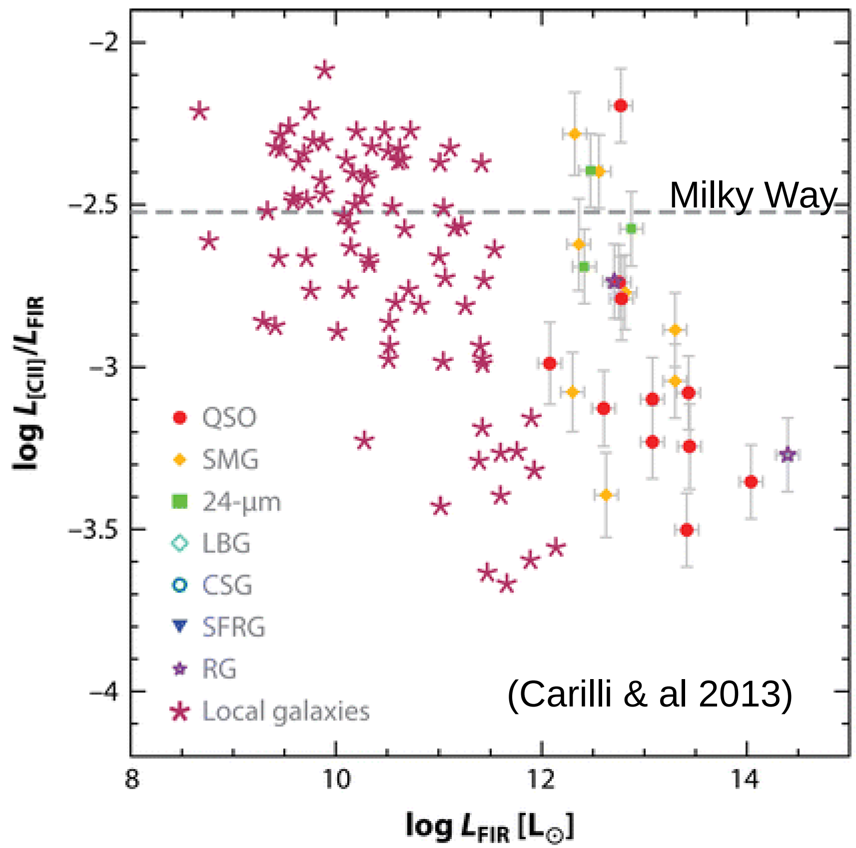

Molecular lines

Chemical[a] formula	Molecule name	Transition	ν/GHz	E_u/K[b]	A_{ij}/s^{-1}[c]
H_2O	ortho-water*	$J_{K_a K_c} = 6_{16} - 5_{23}$	22.235253	640	1.9×10^{-9}
NH_3	para-ammonia	$(J, K) = (1, 1) - (1, 1)$	23.694506	23	1.7×10^{-7}
NH_3	para-ammonia	$(J, K) = (2, 2) - (2, 2)$	23.722634	64	2.2×10^{-7}
NH_3	ortho-ammonia	$(J, K) = (3, 3) - (3, 3)$	23.870130	122	2.5×10^{-7}
SiO	silicon monoxide*	$J = 1 - 0, v = 2$	42.820587	3512	3.0×10^{-6}
SiO	silicon monoxide*	$J = 1 - 0, v = 1$	43.122080	1770	3.0×10^{-6}
SiO	silicon monoxide	$J = 1 - 0, v = 0$	43.423858	2.1	3.0×10^{-6}
CS	carbon monosulfide	$J = 1 - 0$	48.990964	2.4	1.8×10^{-6}
DCO^+	deuterated formylium	$J = 1 - 0$	72.039331	3.5	2.2×10^{-5}
SiO	silicon monoxide*	$J = 2 - 1, v = 2$	85.640456	3516	2.0×10^{-5}
SiO	silicon monoxide*	$J = 2 - 1, v = 1$	86.243442	1774	2.0×10^{-5}
$H^{13}CO^+$	formylium	$J = 1 - 0$	86.754294	4.2	3.9×10^{-5}
SiO	silicon monoxide	$J = 2 - 1, v = 0$	86.846998	6.2	2.0×10^{-5}
HCN	hydrogen cyanide	$J = 1 - 0, F = 2 - 1$	88.631847	4.3	2.4×10^{-5}
HCO^+	formylium	$J = 1 - 0$	89.188518	4.3	4.2×10^{-5}
HNC	hydrogen isocyanide	$J = 1 - 0, F = 2 - 1$	90.663574	4.3	2.7×10^{-5}
N_2H^+	diazenylium	$J = 1 - 0, F_1 = 2 - 1, F = 3 - 2$	93.173809	4.3	3.8×10^{-5}
CS	carbon monosulfide	$J = 2 - 1$	97.980968	7.1	2.2×10^{-5}
$C^{18}O$	carbon monoxide	$J = 1 - 0$	109.782182	5.3	6.5×10^{-8}
^{13}CO	carbon monoxide	$J = 1 - 0$	110.201370	5.3	6.5×10^{-8}
CO	carbon monoxide	$J = 1 - 0$	115.271203	5.5	7.4×10^{-8}
$H_2{}^{13}CO$	ortho-formaldehyde	$J_{K_a K_c} = 2_{12} - 1_{11}$	137.449959	22	5.3×10^{-5}
H_2CO	ortho-formaldehyde	$J_{K_a K_c} = 2_{12} - 1_{11}$	140.839518	22	5.3×10^{-5}
CS	carbon monosulfide	$J = 3 - 2$	146.969049	14.2	6.1×10^{-5}
$C^{18}O$	carbon monoxide	$J = 2 - 1$	219.560319	15.9	6.2×10^{-7}
^{13}CO	carbon monoxide	$J = 2 - 1$	220.398714	15.9	6.2×10^{-7}
CO	carbon monoxide	$J = 2 - 1$	230.538001	16.6	7.1×10^{-7}
CS	carbon monosulfide	$J = 5 - 4$	244.935606	33.9	3.0×10^{-4}
HCN	hydrogen cyanide	$J = 3 - 2$	265.886432	25.5	8.5×10^{-4}
HCO^+	formylium	$J = 3 - 2$	267.557625	25.7	1.4×10^{-3}
HNC	hydrogen isocyanide	$J = 3 - 2$	271.981067	26.1	9.2×10^{-4}

[a] If isotope not explicitly given, this is the most abundant variety, i.e., ^{12}C is C, ^{16}O is O, ^{14}N is N, ^{28}Si is Si, ^{32}S is S
[b] Energy of upper level above ground, in Kelvin
[c] Spontaneous transition rate, i.e., the Einstein A coefficient
* Always found to be a maser transition
** Often found to be a maser transition

CO vs H2

H2 is the most abundant molecula tracing the molecular mass in clouds and plays a key role in excitation, thermal balance, and gas-phase chemistry, but it is a homonuclear linear molecule

- it has no permanent dipole moment
  - -> can be vibrationally excited at high temperatures, observable in MIR, but the warm molecular gas at these temperatures (100-1000K) is only a small fraction (~5%) of the cool molecular gas (Roussel et al. 2007
  - -> dipole rotational transitions have low probability and require high excitation energies (only quadrupole rotational transitions are allowed but very weak)

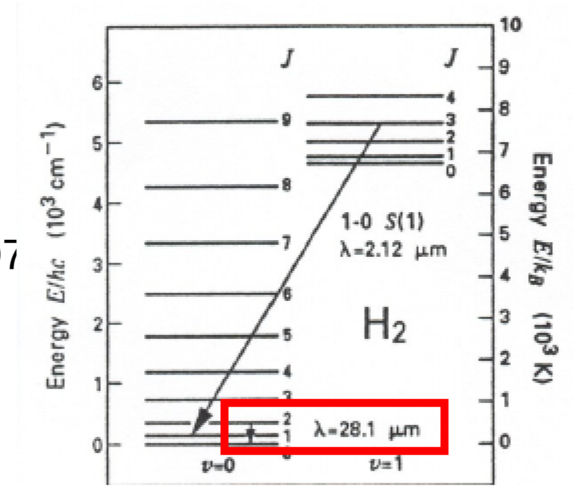

-the excited levels are at high T so under normal interstellar conditions these are not populated except in regions of high excitation (e.g., shocks).

CO is the second most abundant molecula in molecular clouds

- rotational transitions are allowed with critical density ~10^3 cm^{-3} quite common in molecular clouds
- its formation is catalyzed by H2 via $H_2+C^+ \rightarrow CH + CH_2$
  $CH+O_2 \rightarrow CO+H_2$
- rotational transitions are excited by collisions with H2
- J(1-0) transition is at 115.27 GHz
- as it is optically thick its luminosity is a measure of the surface density and allows to estimate virial masses.

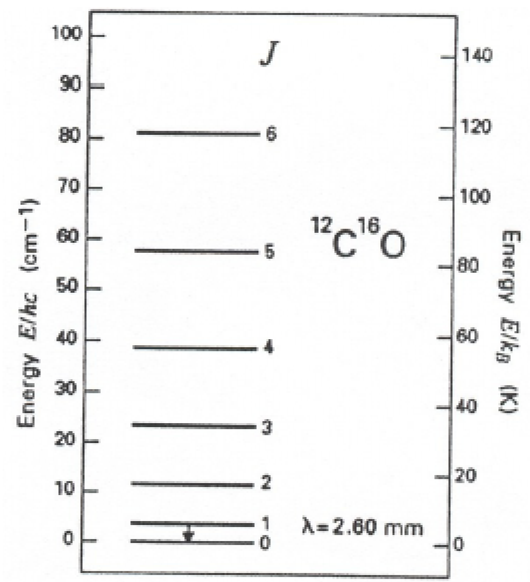

CO vs H2

$$L_{CO} = D^2 \int I_{CO} d\Omega = T_A^*(CO)\Delta v \pi R_C^2 = \left(\frac{3\pi G}{4\rho_C}\right)^{1/2} T_A^*(CO) M_C$$

$$I_{CO} = \int T_A^* dv \qquad \Delta v = \left(\frac{GM_C}{R_C}\right)^{1/2} \qquad \rho_C = \frac{3M_C}{4\pi R_C^3}$$

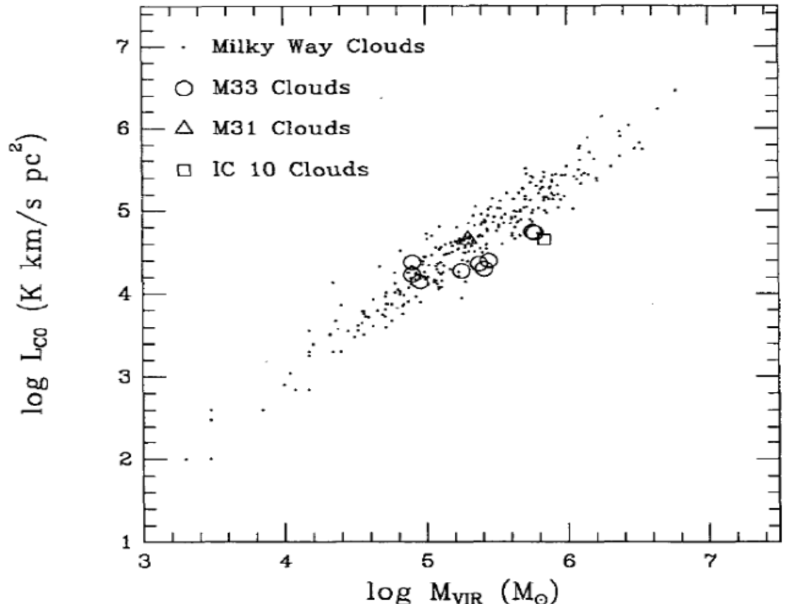

$$M(\mathrm{H_2}) = \alpha L'_{\mathrm{CO}}$$

Indeed, the precise value of the conversion factor depends on the density, temperature and metallicity of the gas

$\alpha \equiv M_{\rm gas}/L'_{\rm CO} = 4.6\ M_\odot\ (\mathrm{K\ km\ s^{-1}\ pc^2})^{-1}$ in MW type galaxies (with increase in low metallicity)

$\alpha \sim 0.8\ M_\odot\ (\mathrm{K\ km\ s^{-1}\ pc^2})^{-1}$ in SMGs and quasar hosts

The difference is due to the fact that CO does not arise in virialized molecular cloud, but also in the warm PDR. Hence **the line emission is due to the total dynamical mass.**
The different values are consistent with a more extended disk-like CO distribution and lower CO excitation in MW type galaxies, compared to more compact morphologies, higher excitation in SMG and QSO.

The star formation law

The star formation law describes how efficiently galaxies turn their gas into stars.
The volume density of star formation is a function of the gas surface density

$$\Sigma_{\rm SFR} = A\ \Sigma_{\rm gas}^{N}$$

According to Kennicutt (1998) N=1.4 (determined empirically).

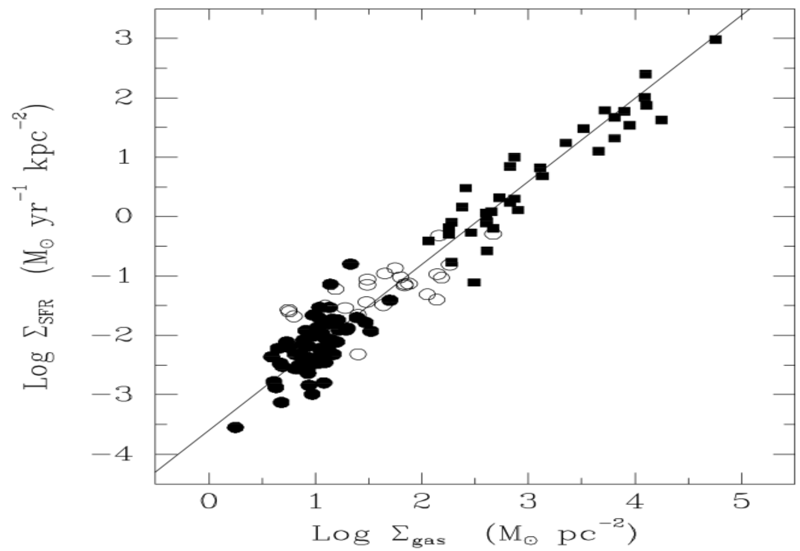

Measurement of surface densities requires resolved observations of galaxies.
The gas density is almost completely due to H2.
Hence, CO is a tracer of the gas surface density
(with all the caveats on the CO vs H2 mass determination)

The SFR is traced by the integrated IR luminosity

Hence, the relation between the

$$\log L_{\rm FIR} = 1.7 \log L'_{\rm CO} - 5.0$$

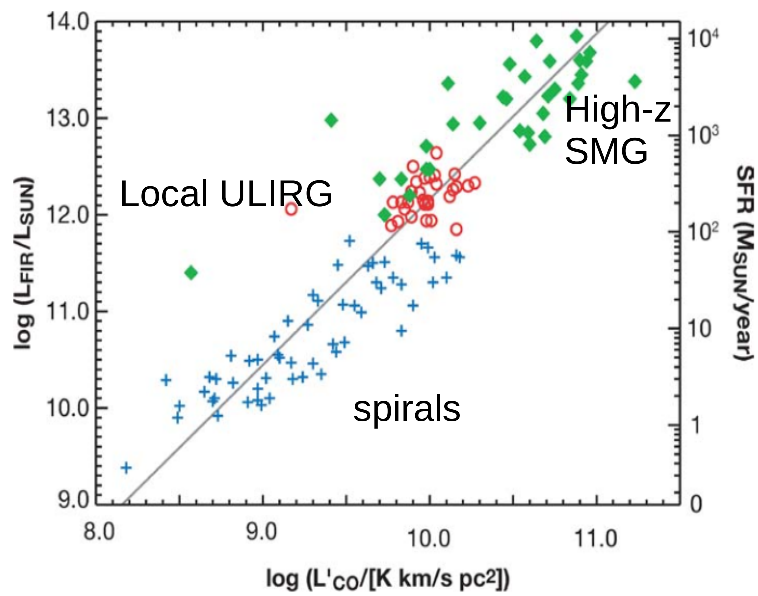

The star formation law

High-z observations suffer of low resolution and so far exploited high-J CO transitions
Including high-z there are two trends:

For starbursts $$\log(L_{\mathrm{IR}}) = 1.37(\pm 0.04) \times (\log L'_{\mathrm{CO}}) - 1.74(\pm 0.40)$$

For MW type galaxies $$\log(L_{\mathrm{IR}}) = 1.13 \times (\log L'_{\mathrm{CO}}) + 0.53$$

The gap arises from similar arguments as for the L_CO-H2 mass relation
Also the time of gas comsumption depends on the α coefficient.

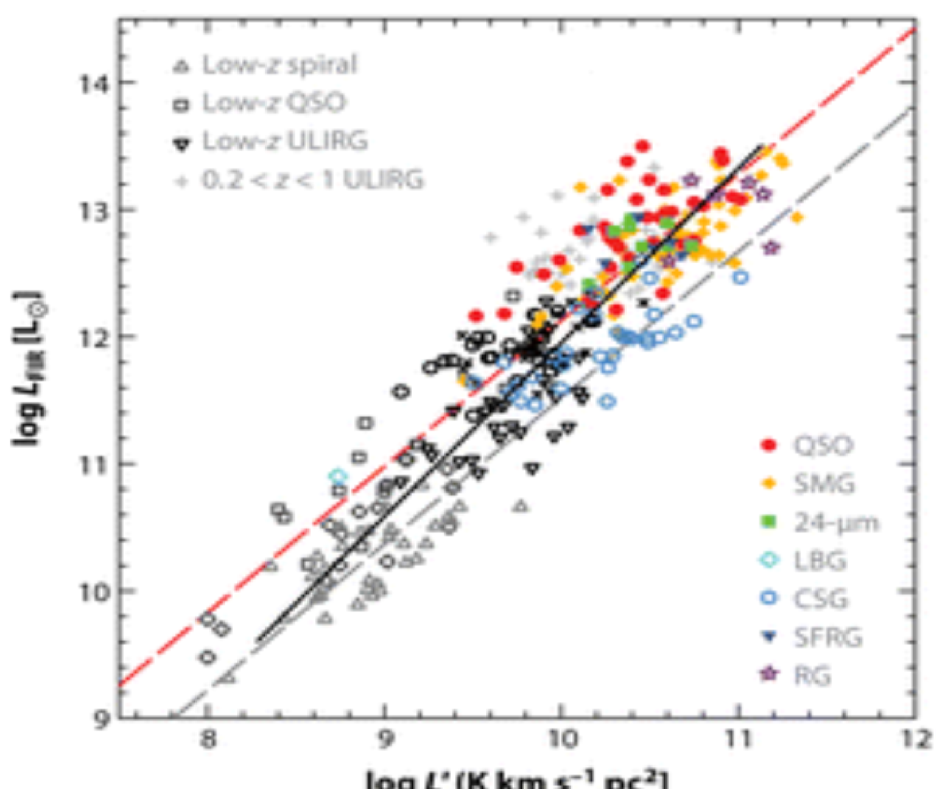

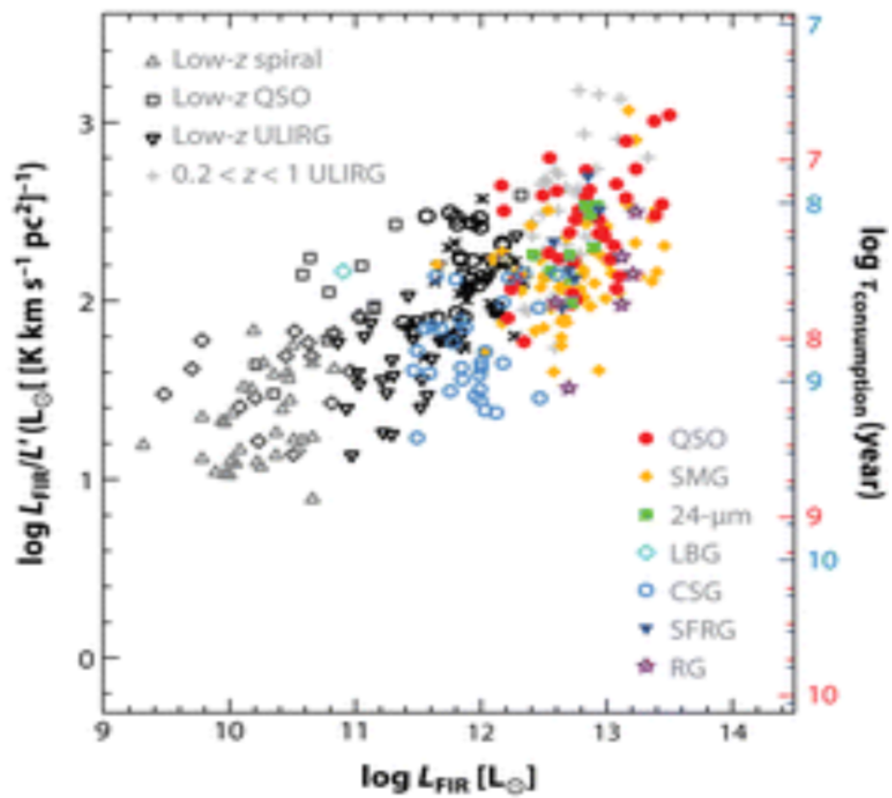

(Carilli & al 2013)

XDRs

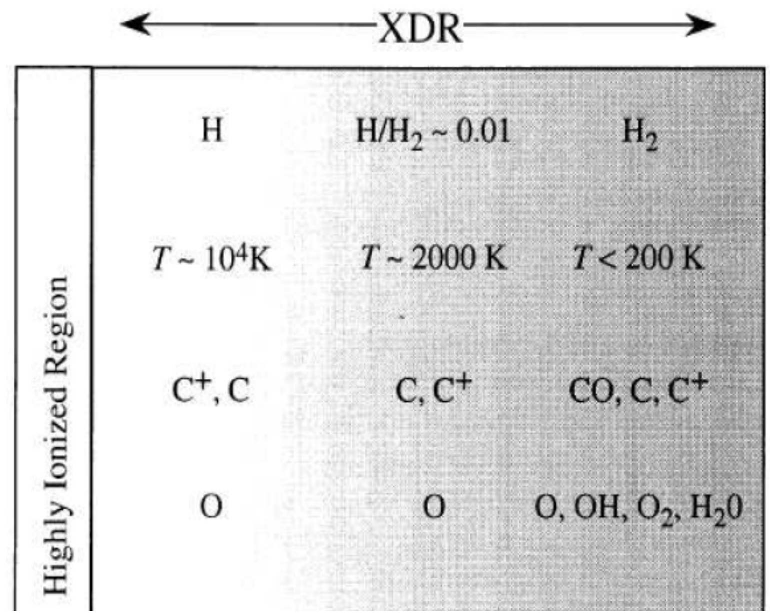

X-rays have a larger penetration depth than UV-photons.

Hence in presence of X-ray sources molecular clouds can be penetrated by radiation and get higher temperature and emissions are different than in PDRs. The regions surrounding X-ray sources are referred as X-ray dominated regions. X-ray sources that are relatively closer to us are young stellar objects (YSO)with protoplanetary disks, and the associated X-ray spectra can form XDRs in some parts of the disks. XDRs are also seen in active galactic nuclei (AGNs) in other galaxies.

Presence of XDR species is a discriminant of AGN activity vs starburst activity.

In XDR there are enhancement of CN and HCN because of high ionization.

This leads to higher ratios of HCN/CO and CN/HCN. They also showed the dependence of HCO+ on the ionization rate, increasing until the peak, then dropping steeply afterwards.

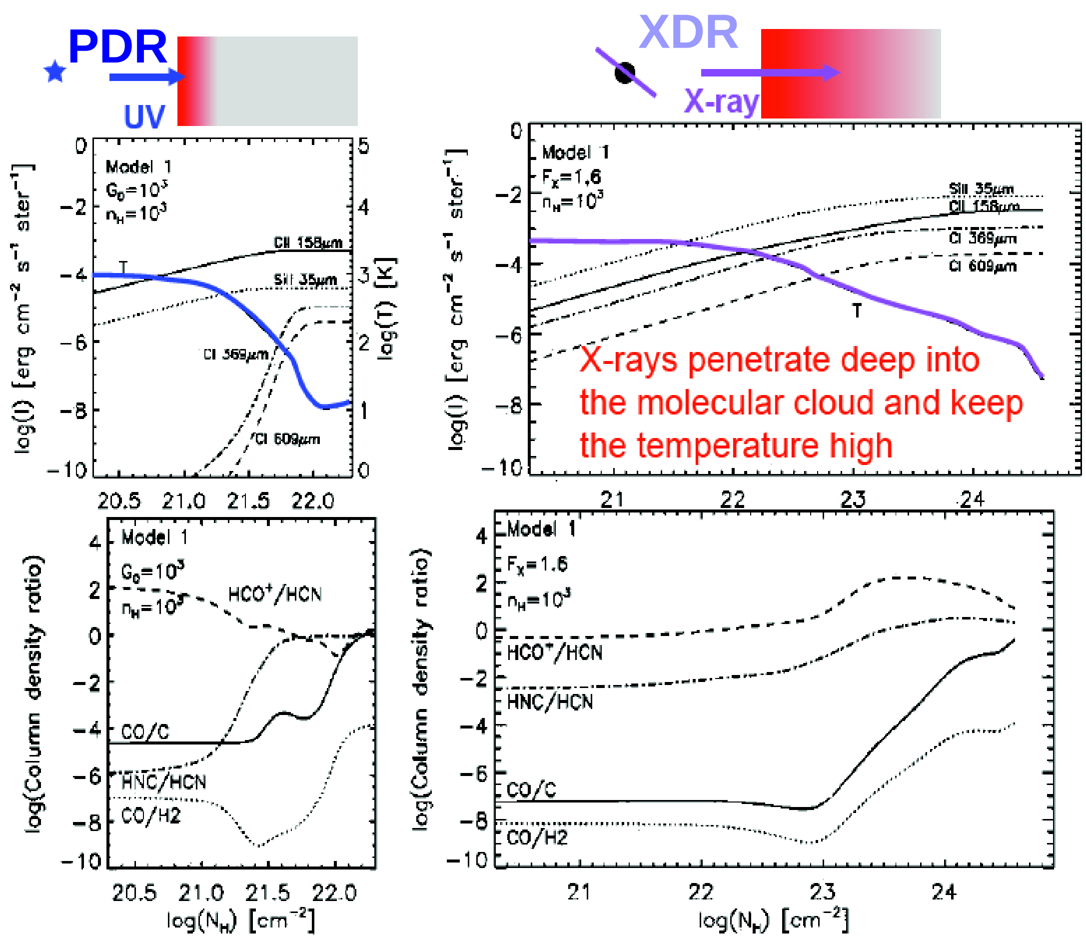

HCN in XDR

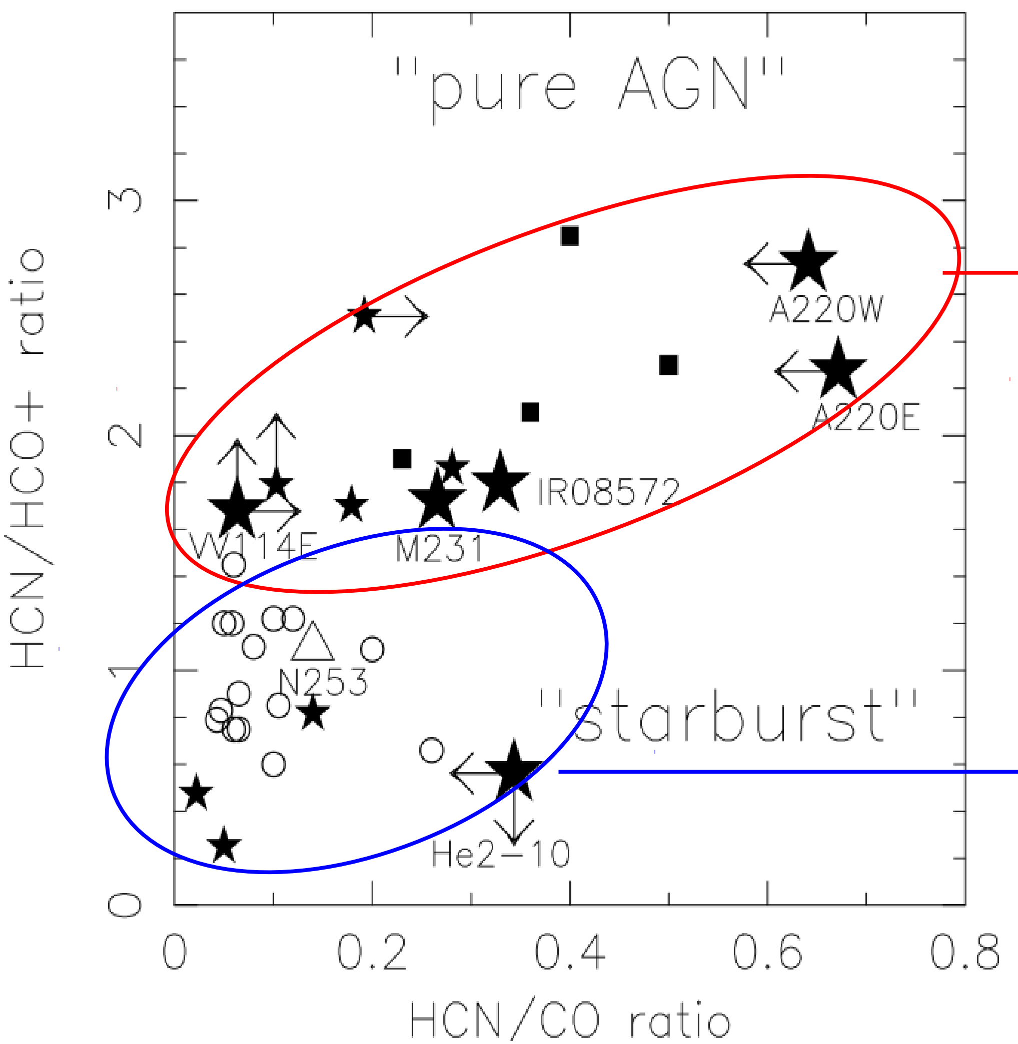

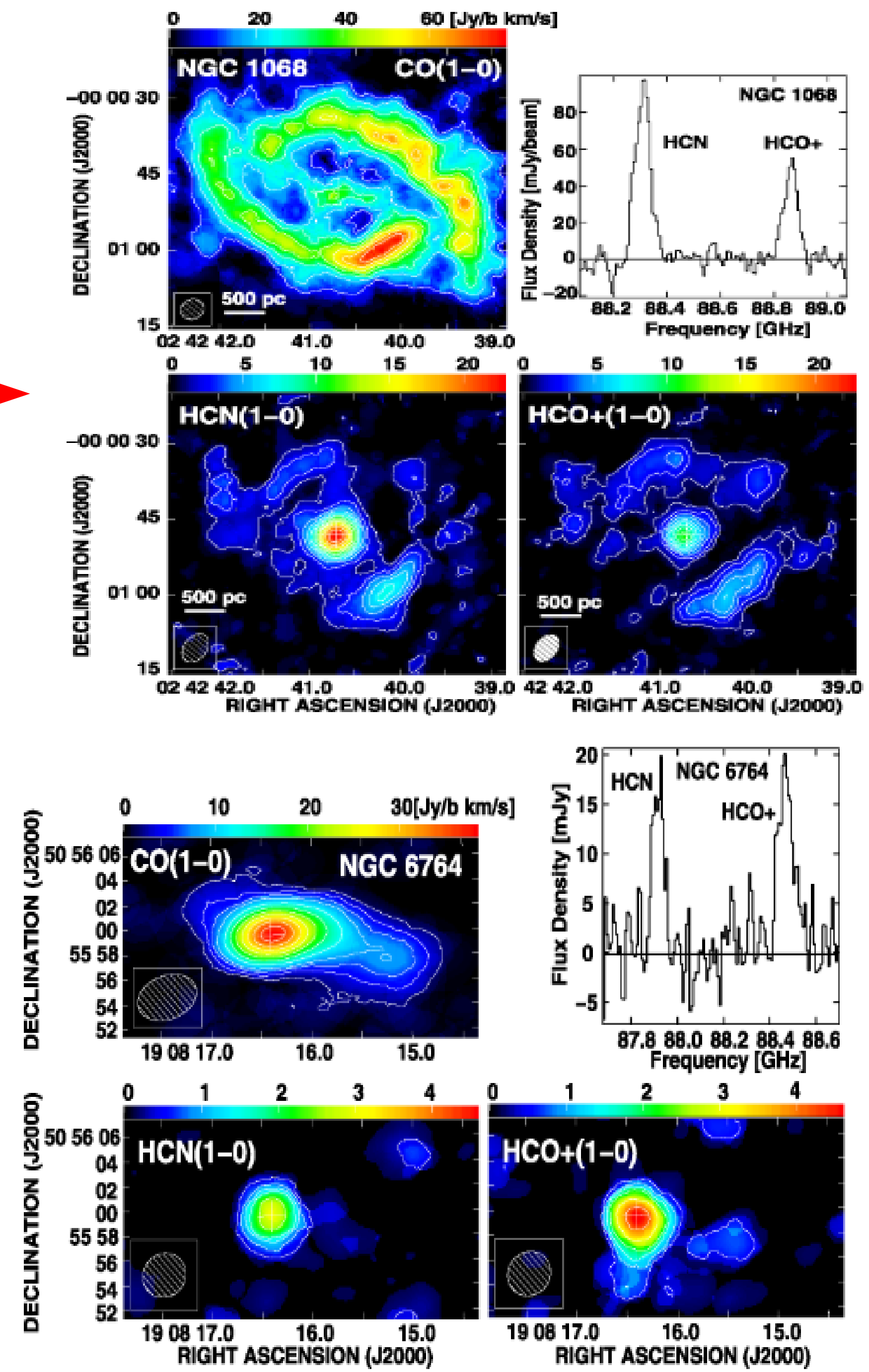

(Khono et al. 2008, Imanishi et al. 2007)

HCN in XDR

Dense gas traced by HCN better correlated with LFIR than CO.
SFE correlated with dense gas fraction.

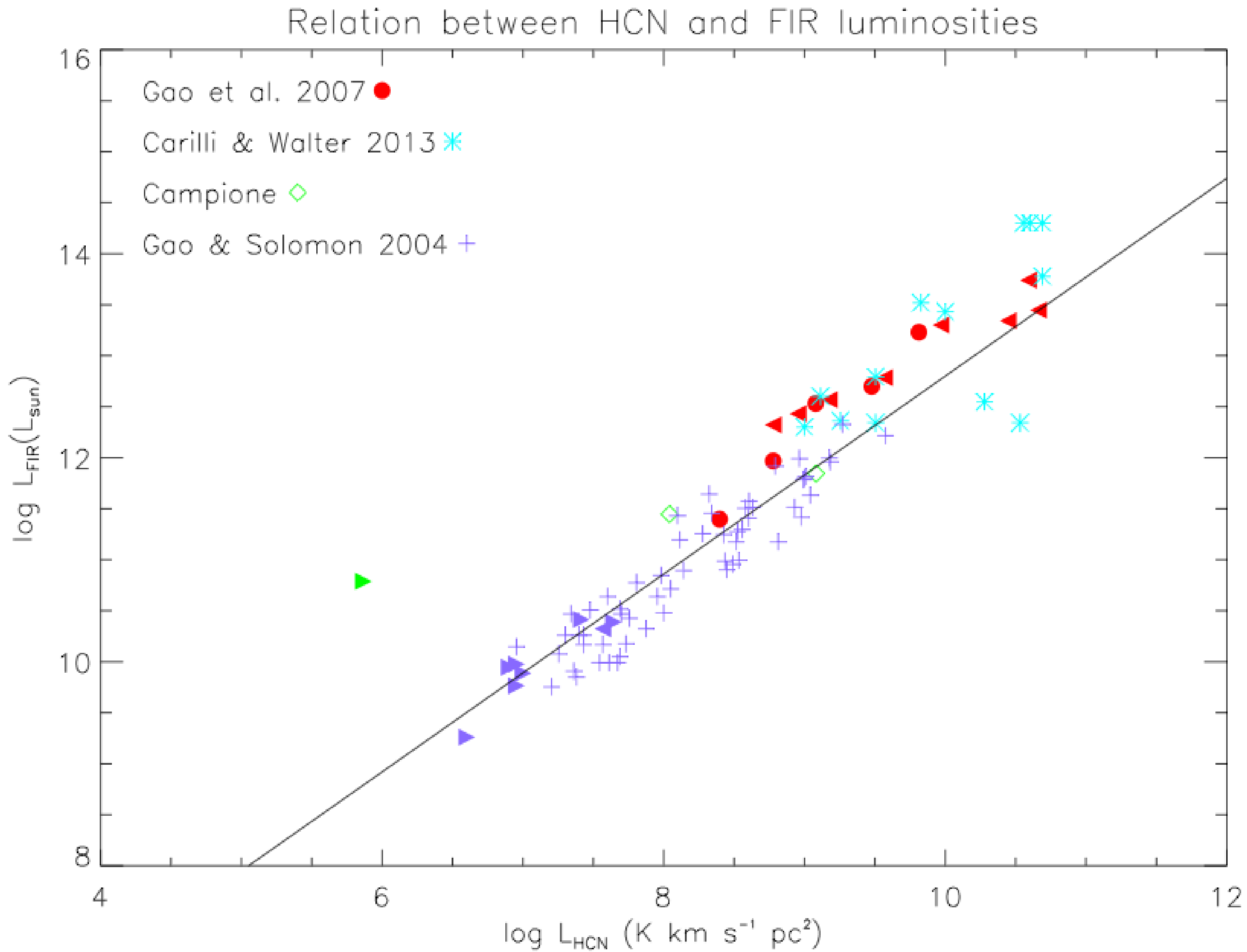

$$\log L_{IR} = 1.00(\pm 0.05) \log L_{HCN} + 2.9$$

(courtesy by Bianchi)

Intensity ratios

Ratios of intensity of different lines are tracer of physical conditions in the clouds
In molecular clouds they are used to derive T, tau, density. E.g. by taking the ratio between same transition of different isotopes of same molecule, or between different transitions of same isotope.
In particular help to distinguish PDR from XDR:

- **PDR intensities depend on surface density, while on column density in XDR.**
- Fine structure emissions are produced on the edge of the cloud, while in the XDR all the cloud contribute.
- Thin lines (CII) are stronger in PDR (because of lower recombination probability), thick lines (CO) are stronger in XDR (because consider all the volume)

- Higher J transition have higher critical densities, so ratios between very different J levels help distinguishing PDR and XDR.
SLEDs allow to distinguish the emitting regions and the properties of the populations.

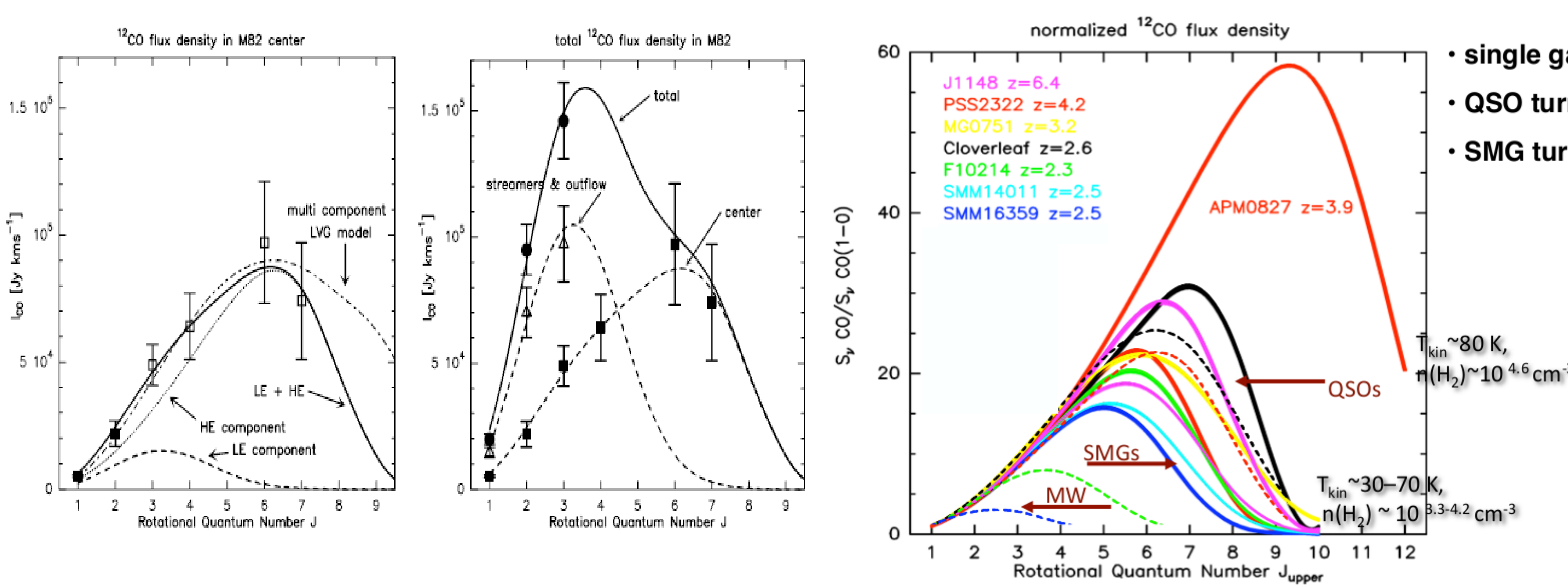

- **single gas component**
- **QSO turnover: J > 6-5**
- **SMG turnover: J ~ 5-4**

Intensity ratios

Ratios of intensity of different lines are tracer of physical conditions in the clouds.
In particular help to distinguish PDR from XDR (i.e. SB galaxies from AGNs):

- PDR intensities depend on surface density, while on column density in XDR.
- Fine structure emissions are produced on the edge of the cloud, while in the XDR all the cloud contribute.
- Thin lines (CII) are stronger in PDR (because of lower recombination probability), thick lines (CO) are stronger in XDR (because consider all the volume)

- Higher J transition have higher critical densities, so ratios between very different J levels help distinguishing PDR and XDR.
  SLEDs allow to distinguish the emitting regions and the properties of the populations.

- HCN/HCO+ discriminate between PDR and XDR
- HNC/HCN are of the order 1(<1) for $N_H>10^{22}$ cm^{-2} ($N_H<10^{22}$ cm^{-2})
  Never exceed 1 in PDR, while can be as high as 1.6 in XDR
- HCN/CO are smaller for XDR than PDR because HCN is boosted in high column density gas and CO is more excited in higher temperature in XDR

XDR are typically more compact in AGN than PDR in SB

Astrochemistry

About 150 different molecules have been detected.

Most interstellar and circumstellar molecules are organic in nature (i.e. dominated by C).
Of the detected species with >6 atoms (ca. 50), 100% are organic even.
Species with >6 atoms are called complex organic molecules (COMs) (Herbst et al. 2009).

COMs have been found basically everywhere
(circumstellar envelopes, outflows, hot/cold/lukewarm cores, etc.)
and different types of sources can be associated with different types of
COMs. No COMs have yet been found in protoplanetary disks though.

Shock chemistry

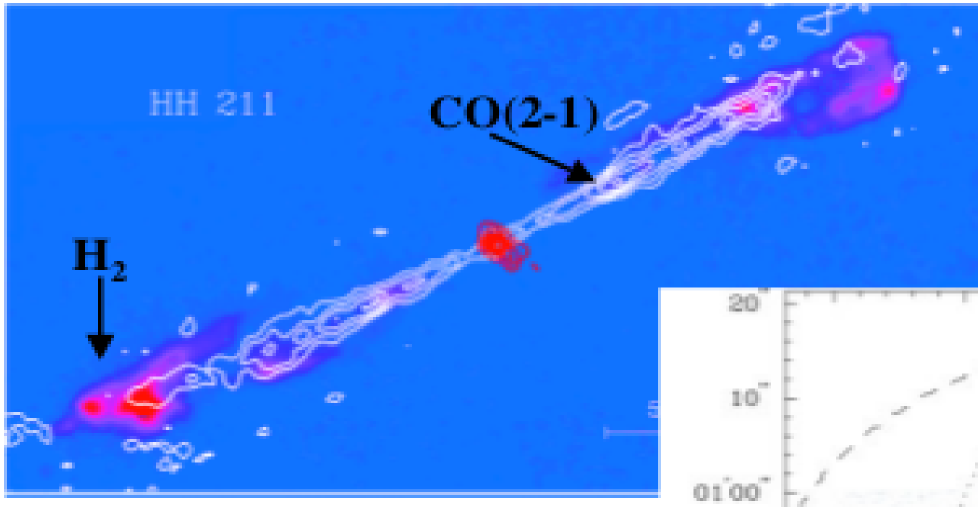

Gueth & Guilloteau (1999)

HH211

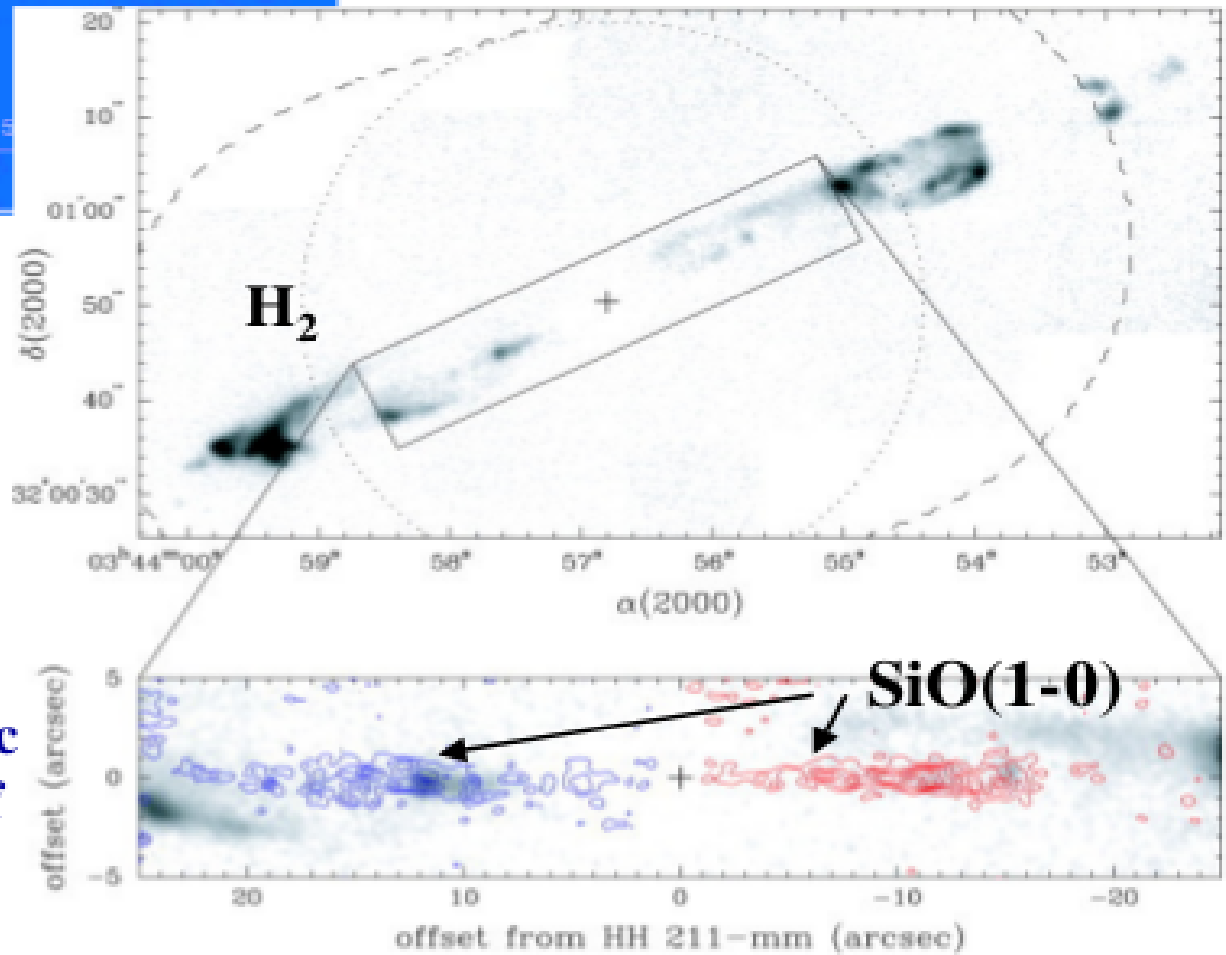

Chandler & Richer (2001)

The heating and compression caused by shocks gives rise to dramatic effects in the chemical composition of the surrounding cloud.

Dissociation, endothermic reactions, sublimation of ices and disruption of grains lead to a shock-chemistry

Shock chemistry

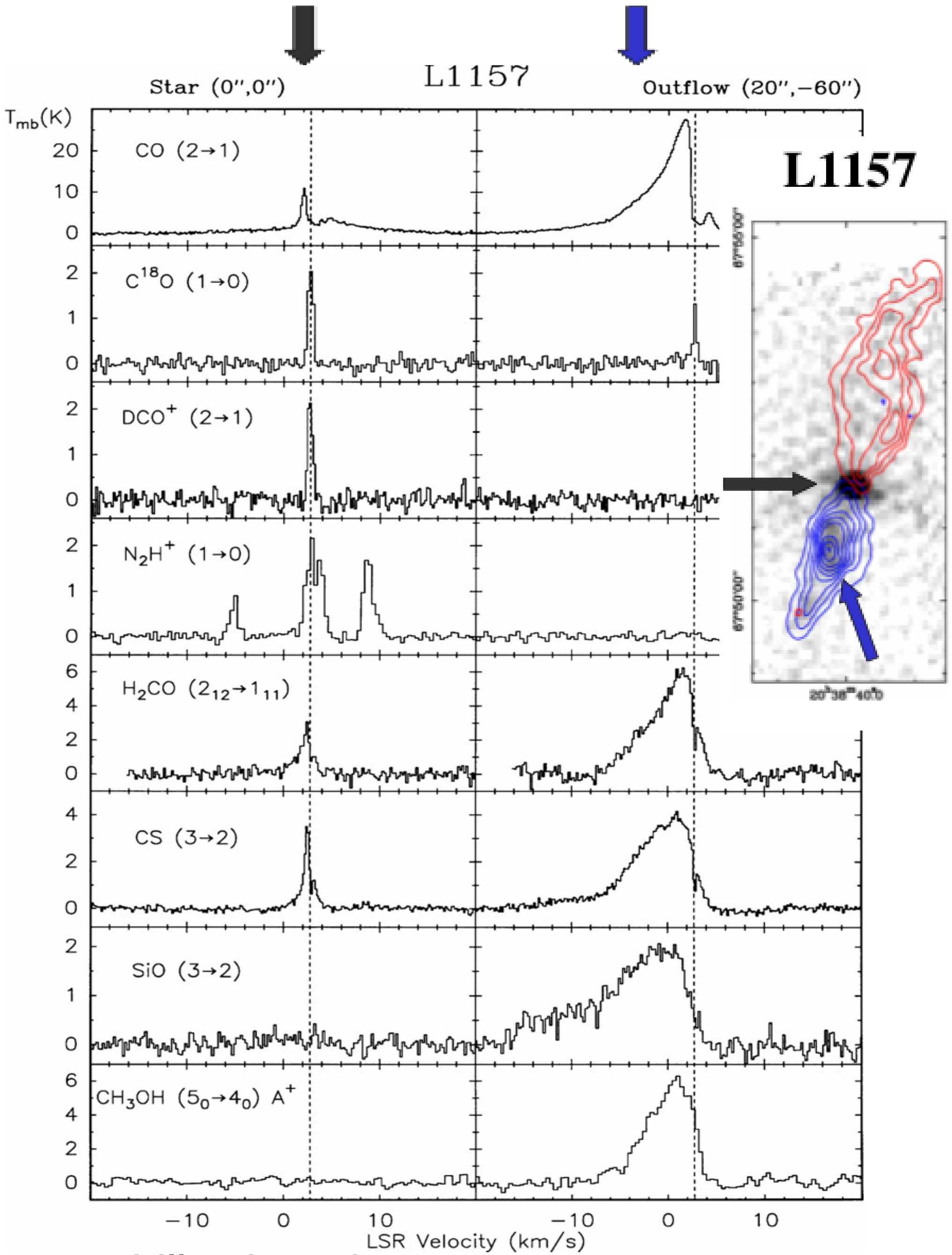

Bachiller (1996)

A mm-line survey toward the L1157 outflow.
The narrow line profiles arise from cold quiescent gas,
Toward the bow shock region the profiles are
dominated by the broad lines associated with
the shock.
DCO+ and N2H+ are only observed toward the cold
gas condensation around the exciting source
SiO and methanol (CH3OH) only trace the hot warm
gas in the shock.
CS and H2CO lines are in both gas components.

The emission of shock-chemistry molecules is seen at
the position of the bowshocks, but SiO emission is
also seen arising from shocks along the highly
collimated molecular outflow.
It seems clear that SiO is a result of the shock
chemistry following the destruction of the refractory
grain cores.

Other molecules such as ammonia and methanol,
which are known to be abundant in the
ice dust mantles, could be directly desorbed from
them. Deuterated species could also be removed from
the grains by grain-grain collisions. The origin
of other molecules such as SO and HCO+ is even
less clear.

Summary

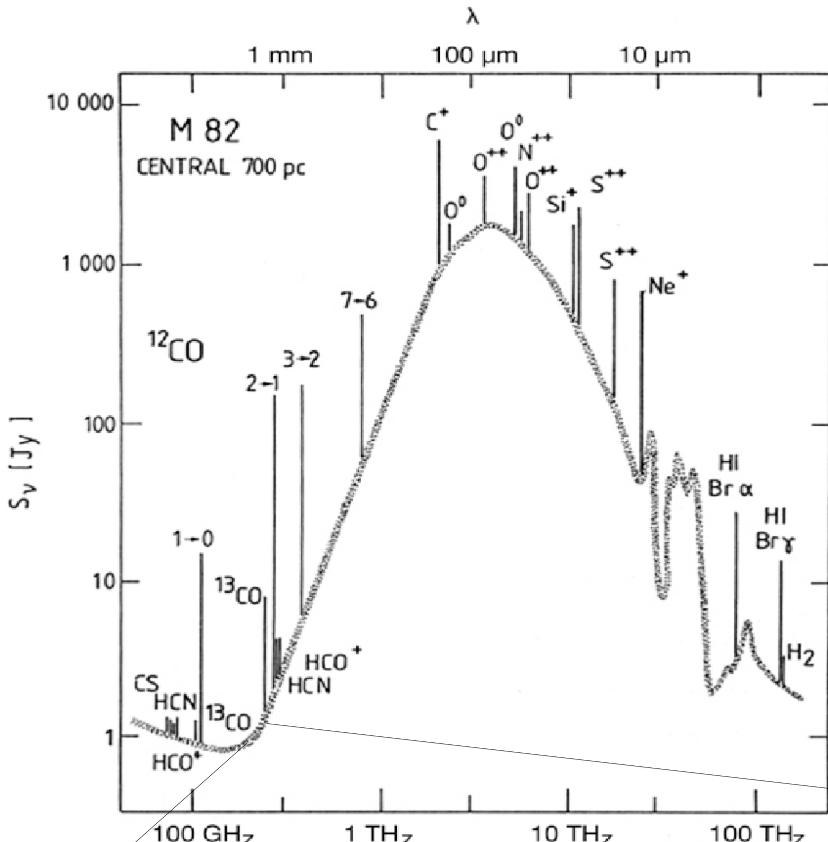

- Continuum is dominated by dust and synchrotron

- CO is the second most abundant molecule after H2
- HCN and HCO+ are high density tracers and relative abundances help distinguish AGN-SB

- CII is the brightest line of nearly all galaxies and PDR tracer
- NII and OII are tracers of cloud metallicity

- Organic molecules are typically associated to young stellar objects
- SiO, CH3OH, H2O are shock tracers